Office of Naval Research
Department of the Navy
Contract Nonr-220(24)

WATER TUNNEL OBSERVATIONS ON THE FLOW PAST A PLANO-CONVEX HYDROFOIL

by
R. B. Wade

Division of Engineering and Applied Science
CALIFORNIA INSTITUTE OF TECHNOLOGY
Pasadena, California

Report No. E-79-6

February 1964

Office of Naval Research
Department of the Navy
Contract Nonr-220(24)

WATER TUNNEL OBSERVATIONS ON THE FLOW PAST A PLANO-CONVEX HYDROFOIL

by

R. B. Wade

Division of Engineering and Applied Science
California Institute of Technology
Pasadena, California

Report No. E-79-6
February 1964

Approved by:
A. J. Acosta

I. Abstract

Experimental results of the performance of a plano-convex hydrofoil under non-cavitating and cavitating conditions are presented. Lift, drag and moment coefficients are given as a function of the cavitation number, together with the behavior of the cavity length.

Some unsteady effects occurring under cavitating conditions are also considered. In this region of cavitation the magnitude of the force oscillations together with the fluctuation of the cavity length are presented. The frequency of these oscillations and the general behavior of the cavity are discussed.

II. List of Symbols

t = thickness of hydrofoil

c = chord length

s = span

R = radius of circular surface of model

ℓ = cavity length

λ = distance of center of pressure from leading edge

α = angle of attack, degrees

A = plan form area = (s x c) ft^2

ρ = density of water, slugs/cu ft

V = tunnel velocity, ft/sec.

p = corrected tunnel static pressure, p. s. i.

p_k = measured cavity pressure, p. s. i.

p_v = vapor pressure of water, p. s. i.

L = lift force on model, lb

D = drag force on model, lb

M = moment on model, lb in

K = corrected cavitation number = $\dfrac{p - p_k}{\frac{1}{2}\rho V^2}$

K_v = cavitation number based on vapor pressure
= $\dfrac{p - p_v}{\frac{1}{2}\rho V^2}$

C_L = lift coefficient = $\dfrac{L}{\frac{1}{2}\rho V^2 A}$

C_D = drag coefficient = $\dfrac{D}{\frac{1}{2}\rho V^2 A}$

C_M = moment coefficient = $\dfrac{M}{\frac{1}{2}\rho V^2 A c}$ about the mid-chord point

f = frequency of oscillations, c. p. s.

III. Introduction

With the advent of hydrofoil boats and the demand for higher speed pumps and propellers the study of the performance of hydrofoil sections under cavitating conditions has become essential. The knowledge of the characteristics of these hydrofoils under varying cavitation becomes a necessity with the designer. Furthermore, important unsteady effects become apparent in a certain regime of cavitation which affects the performance of the hydrofoil to a marked extent and which could lead to deleterious effects in any of the above applications.

In propeller design extensive use has been made of plano-convex hydrofoils, viz;hydrofoils with a flat under-surface and a circular-arc suction surface. It was therefore decided to conduct the tests on such a section. Since this type of hydrofoil has sharp leading and trailing edges the cavity usually springs from the leading edge due to the large suction pressure occurring there. This condition is not always met, however. At low angles of attack, below 4^{o} for the section tested, the cavity appears downstream of the leading edge on the suction surface. The emphasis of the present tests was placed on angles of attack greater than 4^{o}.

Thus in the range tested the separation point of the cavity remained fixed. This condition gave rise to a more predictable flow configuration than would otherwise have occurred if the leading

edge were rounded, in which case the forward separation point of the cavity is not fixed.

IV. Experimental Procedure

The tests were conducted in the High Speed Water Tunnel in the Hydrodynamics Laboratory.[1]* The model used, as previously mentioned, was a plano-convex hydrofoil, the dimensions of which are shown in Figure 1. The 14 in. diameter, axisymmetric section of the tunnel was converted to an approximately, 14 in. by 3 in. two-dimensional rectangular section, by the use of two inserts, as explained in Ref. 2.

The model was mounted on a base plate (see Figure 1) which in turn was bolted to the spindle of the force balance so that the plate was set flush with the tunnel wall. A circular gap of approximately 0.020 in. was left between the disk and the wall. The force balance and readout equipment provided a means of measuring the lift, drag and moment on the hydrofoil. This set-up is explained in detail in Ref. 3.

The end gap between the model and the facing wall was adjusted to 0.005 in. and kept approximately at this value throughout the experiment. Although this end gap did vary slightly it was

---

* Numbers in parentheses refer to reference number in Section XIII

found that the variation of the forces with end gap over a range of 0.005 in. to 0.0105 in. was less than 5 percent for the lift and drag and negligible for the case of moment. These runs were conducted for fully wetted flows at several angles of attack. During a test run the variation of the end gap, due to the difference in pressure between the working section and the dead water region on the viewing side of the tunnel wall was never greater than $\pm$ 0.004 in. hence this effect was sufficiently small as to be ineffectual. Similar results were obtained in Ref. 2, although a somewhat larger drag variation was obtained due probably to the greater thickness of the model.

The readings for the forces were corrected for zero shift of the gage readings due to tunnel static pressure variation and for the tare forces on the mounting disk. These tare forces, although small in the case of lift and negligible in the case of moment comprise, under certain circumstances, as much as 30 percent of the total drag force. The results of these tests are shown in Appendix I. The method of obtaining these results, by mounting the model from the opposite wall of the tunnel is described in Ref. 2.

The velocity, V and hence the dynamic head, $1/2\rho V^2$ were determined by measuring the pressure drop across the piezometer ring at the 5 ft. diameter circular section of the tunnel prior to the tunnel nozzle and the two-dimensional section. This pressure reading was recorded on the force read out console.

The static pressure in the tunnel was measured in the two-dimensional section by means of a mercury manometer.

The cavity pressure was recorded with respect to working section static pressure by means of a mercury manometer, the reading was corrected for the fact that one leg of the manometer contained water and the other leg air. The cavity pressure was obtained by means of a pressure tap located 0.2 in. behind the leading edge, on the suction face of the hydrofoil at mid-span. Due to the frothy nature of the cavity, water tended to enter the pressure line from the cavity to the manometer thus blocking it. To ensure a correct reading of the cavity pressure, this line was kept clear of water by constant purging with a small amount of air.

Due to the dimensions of the working section used all pressure taps located in the working section are influenced by the circulation around the model. The question then arises as to what does one call the true working section static pressure or ultimately what is the pressure corresponding to a point far away from the model.

It was found necessary, therefore, with the experimental procedure used to correct all the above mentioned pressure measurements taken in the working section for the model interference. This is necessary as all the force coefficients and cavitation numbers should be based on this pressure.

The method adopted for applying this model interference correction is explained in Appendix II.

The test runs were taken at a constant angle of attack for a fixed velocity, V. The tunnel static pressure was then varied in successive steps to obtain different cavitating conditions. The readings on the console were recorded with an electrically operated 35 mm recording camera. The state of cavitation on the hydrofoil was also recorded photographically from the side and in plan view. From these latter photographs, the cavity length could be ascertained as a function of the cavitation number.

The experimental set-up is shown in Figure 2. Figure 3 shows a view of the force balance attached to the tunnel.

The series of tests conducted, covered a range of angles of attack of 4^{o} to 10^{o} over a range of velocities from 15 feet per second to 40 feet per second.

For each run the lift, drag and moment coefficients were calculated. These being defined according to Section II as

$$C_L = \frac{L}{\frac{1}{2}\rho V^2 A} \quad ; \quad C_D = \frac{D}{\frac{1}{2}\rho V^2 A}$$

$$C_M = \frac{M}{\frac{1}{2}\rho V^2 Ac}$$

The cavitation number based on measured cavity pressure and based on water vapor pressure were also determined, viz.

$$K = \frac{p - p_k}{\frac{1}{2}\rho V^2} \qquad K_v = \frac{p - p_v}{\frac{1}{2}\rho V^2}$$

the symbols being defined in Section II.

Finally, the cavity length-to-chord ratio was determined from the 35 mm photographs taken of the cavity on the hydrofoil.

For the fully-wetted runs, the velocity and tunnel pressure were maintained constant and the angle of attack varied over the range of interest viz. -4^{o} to 15^{o} in steps of 15 minutes of arc. This was repeated for several velocities to give a range of Reynold's numbers.

In all the above readings no account was made for tunnel interference effects such as wall interference effects, model and wake blockage effects and static pressure gradient effect down the working section.

It is well known[4],[5] that when the cavity length is in the neighborhood of the chord length an unsteady phenomenon becomes apparent and the forces on the hydrofoil fluctuate violently as does the cavity itself. This unsteady region persists over a range of cavity length to chord length ratios of approximately 0.6 to 1.2. On either side of this region, namely, in the partially cavitating and fully cavitating regions, the flow is relatively steady. To study this region of unsteady flow more fully it was necessary to make use of the output of a semi-conductor strain gage embedded at the root of the hydrofoil, flush with the flat surface and situated at mid-chord. It was necessary to make use of a strain gage as the response of the force balance was completely inadequate to be of any use in measuring the unsteady forces on the model.

The output of this strain gage was recorded by means of a recording oscillograph using photo-sensitive paper. This output afforded a means of measuring the fluctuating normal force component on the model together with its frequency.

In conjunction with the strain gage a high speed motion picture camera running at approximately 1,900 frames per second was used to photograph the oscillating cavity. By analyzing film strips frame-by-frame a time history of the cavity growth could be determined. The output of the strain gage was also recorded on the film as a fluctuating light spot which, together with two calibrating marks, enabled the time history of the force to be determined. Several film strips were assembled into a short sound motion picture* which makes it easier to visualize this non-steady cavitation process.

From this unsteady data, a preliminary idea of the salient points governing this region of cavitation could be obtained.

---

* The film entitled "Some non-steady Effects in Cavity Flows", Report No. E79.5, may be borrowed from the Office of Naval Research, Code 438, Dept. of the Navy, Wash. 25, D.C. or the Hydrodynamics Laboratory, Karman Laboratory of Fluid Mechanics and Jet Propulsion, California Institute of Technology, Pasadena, Calif.

V. Experimental Results

A selection of the test points obtained from the experiment are tabulated in the Tables at the back of this report. These results cover the complete range of velocities and angles of attack used. The lift, drag and moment coefficients are given and in the case of cavitating flow the cavitation number, as measured and based on vapor pressure are listed. Space limits the complete set of the data to be given.

To determine how consistently the cavity pressure, or cavitation number, could be recorded and how this reading compared with that based on vapor pressure a plot of K against K_v was made, for varying velocities and angles of attack. As seen in Figure 4, this reading is quite repeatable. The discrepancy between the two readings increases with increasing cavitation number. It will be noted that the cavity pressure is always higher than the vapor pressure. This result is to be expected as the existence of gases in solution together with impurities in the water would cause the formation of bubbles and so cavities at a higher pressure than the vapor pressure. These results also check with those obtained previously.[2]

Firstly, let us consider the fully wetted characteristics of the hydrofoil. In Figure 5, we see the lift, drag and moment coefficients plotted against angle of attack, α. The points are shown for a Reynolds number range of from 0.46×10^6 to 0.75×10^6.

Over this range there is very little significant change in any of the force coefficients.

It is seen that at 1^{o} angle of attack there is a slight stalling effect in the lift curve with a corresponding increase in the drag. This effect is characteristic of certain sharp nose aerofoils and is due to the type of boundary layer separation occurring on the foil.[6],[7],[8] This wave in the lift curve comes about because the laminar separation of the boundary layer at the leading edge and subsequent reattachment forms a small turbulent "bubble". This bubble effectively reduces the high suction peak causing a drop in lift. On further increase in angle of attack the bubble grows rearward until a completely turbulent boundary layer is achieved. This hump in the lift curve can be removed by increase in Reynolds number to approximately 6×10^{6} or by increasing the nose surface roughness, thus stimulating a turbulent boundary layer. These effects are discussed in detail in the above references. The lift slope below this hump is less than 2π but slightly larger than the slope above the hump.

Figures 6 and 7 show respectively the variation of the lift to drag ratio and the center of pressure location with angle of attack. The kinks in these curves at 1^{o} being due, once again, to the boundary layer separation.

For cavitating flow the values of the force coefficients as a function of the measured cavitation number are shown in Figures

8, 9, 10 and 11, each graph being for a different angle of attack. The photographs indicate the degree of cavitation occurring on the hydrofoil at a few different cavitation numbers. These locations are marked on the graphs.

In Figures 12, 13, 14 and 15 are shown graphs of the ratio of cavitation number to angle of attack as a function of cavity length to chord ratio. These points were obtained from the 35 mm photographs taken of the cavity for each data point. The dark points are those occurring in the unsteady flow regime previously mentioned. As can be seen the unsteady region occurs over a region of approximately 0.6 ℓ/c, to 1.2 ℓ/c, regardless of angle of attack. This region of unsteadiness has been indicated on the graphs of the force coefficients as well and the region again represented by dark points.

In this region of cavitation the forces are fluctuating violently and the points shown plotted are those recorded by the force balance. These readings are somewhat meaningless as the force balance frequency response is completely inadequate to react to the vibrating force. However, the curve has been drawn to indicate, in perhaps a rather misleading way, the general trend of the forces in this region.

In Figures 12, 13, 14 and 15 are shown theoretical curves obtained by the use of linearized theory for cavity flows in the regions of full cavitation[9] and partial cavitation[10] on a <u>flat plate</u> hydrofoil. We see that for fully cavitating flow the agree-

ment is better than for the partial cavitating case. This, however, is to be expected since in the former case the hydrofoil acts exactly like a flat plate whereas in partial cavitation, camber and thickness effects play a role. Furthermore, it is seen that agreement is better at the lower angles of attack which is also to be expected, as the linearized theory is based on the assumption that the angle of attack is a small parameter.

In Figure 16, is plotted the polar diagram for the section. In Ref. 11 experimental results on a similar section were carried out in non-cavitating and cavitating conditions, for angles of attack up to 5^{o}. The cavitation number in these experiments is based on vapor pressure and hence a direct comparison of the data cannot be applied too meaningfully. Furthermore, the thickness ratio in this experiment was 7.35 percent as compared with 7 percent in the present case. The results, however, show quite a favorable agreement in the common region covered by both investigations, viz from 4^{o} to 5^{o} angle of attack.

The results of the investigation into the unsteady region of cavitation are given in Figures 17, 18 and 19. In Figure 17, is plotted the time variation of the fluctuating normal force component as a percentage of its mean value. The variation of cavity length to chord length ratio is also shown. These readings are taken in the region of maximum oscillation, for a given angle of attack of 6^{o} and velocity of 27 feet per second, the cavitation number being

0.90. These results were obtained from the high speed motion picture camera, taking frame-by-frame measurements of the cavity length and force amplitude. It will be seen from this diagram that the force fluctuation is of the order of $\pm$ 10 percent of its mean value and is in phase with the cavity oscillation. The average frequency of this run is 16 cycles per second.

The behavior of the cavity during each cycle is of interest. As the cavity length increases from its minimum value there is a corresponding increase in the force. During this process a re-entrant jet forms at the rear end of the cavity, gradually filling it with foam and causing a vortex type motion within the cavity. On reaching the end of the foil the cavity surface becomes uneven and irregular and there is a decrease in the force. Small vortices may be shed from the end of the cavity causing small fluctuations in the force as it decreases. The vortex motion eventually breaks up the cavity causing a large vortex to be shed, reducing the cavity length abruptly and reducing the force to its minimum value. The cycle is then repeated.

In Figure 18, these effects are presented in a slightly different form. Here we have the percentage force change, from its minimum value during the oscillation, as a function of cavity length to chord ratio for the same parameters as above. The arrows indicate the direction in which the curve is traversed during a cycle. The outer loop represents the main cycle of events while the inner

loop corresponds to a secondary oscillation which sometimes occurs as the cavity grows.

The final figure, Figure 19, shows the reduced frequency (fc/V) of the oscillations based on chord length and tunnel velocity. The points shown plotted represent an average of a number of readings obtained from the oscillograph print-outs. The cavitation numbers are the average values during the phase of maximum oscillation. Quite a bit of scatter occurred and these curves should be viewed with some reservation. However, it does seem conclusive that the frequency of oscillation increases with attack angle. Furthermore, the reduced frequency is seen to be essentially independent of velocity which suggests that the frequency of oscillation is not strongly dependent on the rigidity of the surrounding tunnel structure. There is the basic question, however, of the effect of the tunnel (and flow) "compliance" and its effect on such transient cavity flows as described herein which has not yet been answered. For example, if the tunnel were perfectly rigid and if there were no free surfaces other than that of the cavity itself, then an infinite pressure difference (in an incompressible medium) would be required to create the changing cavity volume. The tunnel is compliant however. Numerous pockets of vapor collect in the diffusor and from the photographs (Figs. 8(b) to 11(b)) it can be seen that there are entrained vapor-air bubbles in the flow. All of these evidently provide the cushion for the fluctuating cavity volume.

The lack of an appreciable phase change between the force and cavity length (Fig. 17) suggests that possible inertial effects of the fluid in the tunnel circuit or tunnel rigidity are not large.

We do not know at the present time whether or not the results presented herein on these non-steady effects occur in the presence of a neighboring free surface or on three-dimensional partially cavitating hydrofoils. We would speculate, however, that they do although it is clear that further experimentation is necessary before these points can be settled.

VI. Conclusions

The performance characteristics of a plano-convex hydrofoil have been given for non-cavitating and cavitating flows. The behavior of the lift, drag and moment on the hydrofoil is presented. It is seen that this range of cavitation can be divided up into three regimes; the partially cavitating region, the fully cavitating region and a region of unsteady flow, when the cavity is in the neighborhood of the chord length.

In the partial and fully cavitating regions the forces are steady and are well defined in terms of the cavitation number and angle of attack. The unsteady zone, however, the forces are unsteady and the cavity fluctuates violently. The fluctuating normal force on the hydrofoil measured in the present experiments has

an amplitude variation of ± 10 percent of its mean value in this region. The reduced frequency of the force oscillations appears to be a function principally of the angle of attack. Reduced frequencies based on chord length and tunnel velocity are in the range of 0.10 to 0.20 for angles of attack of 10^{o} or less and for the tunnel velocities used (below 40 feet per second).

The cavity fluctuations are in phase with the force oscillations and the variation in cavity length is of the order of 0.6 percent to 1.2 percent of the cavity length to chord length ratio.

The present investigations on the unsteady region of the cavitation on a hydrofoil are of a preliminary nature, the aim being to acquire some information on the processes involved and to obtain a general qualitative and quantitative picture of the unsteady phenomenon. Future work on tunnel boundary and free surface effects is envisaged.

VII. Acknowledgments

The participation of all the members of the Hydrodynamics Laboratory Staff, during the course of this experimental investigation is gratefully appreciated. In particular the help of Messrs. H. Hamaguchi, J. Brentjes and C. Eastvedt is acknowledged. The author wishes to thank Dr. A. J. Acosta for his constant advice and encouragement at all times. Thanks are due to Miss Cecilia Lin for the preparation of the Figures.

VIII. References

1. Knapp, R.T.,; Levy, J.; O'Neill, J.P.; Brown, F.B.; "The Hydrodynamics Laboratory of the California Institute of Technology", Transactions of A.S.M.E., Vol. 70, No. 5, pp 437-457, (1948)

2. Kermeen, R.W.; "Water Tunnel Tests of NACA 4412 and Walchner Profile 7 Hydrofoils in Non-Cavitating and Cavitating Flows", California Institute of Technology, Hydrodynamics Laboratory, Report No. 47-5, (1956)

3. Hotz, G.M.; McGraw, J.T.; "The High Speed Water Tunnel Three-Component Force Balance", California Institute of Technology, Hydrodynamics Laboratory, Report No. 47-2, (1955)

4. Meijer, M.C.; "Some Experiments on Partly Cavitating Hydrofoils", International Shipbuilding Progress, Vol. 6, No. 60, (1959)

5. Parkin, B.R.; "Experiments on Circular Arc and Flat Plate Hydrofoils in Non-Cavitating and Full Cavity Flows", California Institute of Technology, Hydrodynamics Laboratory, Report No. 47-6, (1956)

6. Williams, D.H.; Brown, A.F.; Miles, C.J.W.; "Tests on Four Circular-Back Aerofoils in the Compressed Air Tunnel", A.R.C. Technical Report R. and M. No. 2301, (1948)

7. McCullough, G.B.; Gault, D.E.; "Boundary Layer and Stalling Characteristics of the NACA 64A006 Airfoil Section", NACA TN 1923, (1949)

8. Carrow, D.D.; "A Note on the Boundary Layer and Stalling Characteristics of Aerofoils", Aeronautical Research Council, C.P. No. 174, (1950)

9. Wu, T.Y.; "A Note on the Linear and Non-Linear Theories for Fully Cavitating Hydrofoils", California Institute of Technology, Hydrodynamics Laboratory, Report No. 21-22, (1956)

10. Acosta, A.J.; "A Note on Partial Cavitation of Flat Plate Hydrofoils", California Institute of Technology, Hydrodynamics Laboratory, Report No. E-19.9, (1955)

11. Walchner, O.; "Profilmessungen bei Kavitation", Hydromechanische Probleme des Schiffsantriebs, edited by Kempf, G. and Foerster, E., (1932), pp 256-267

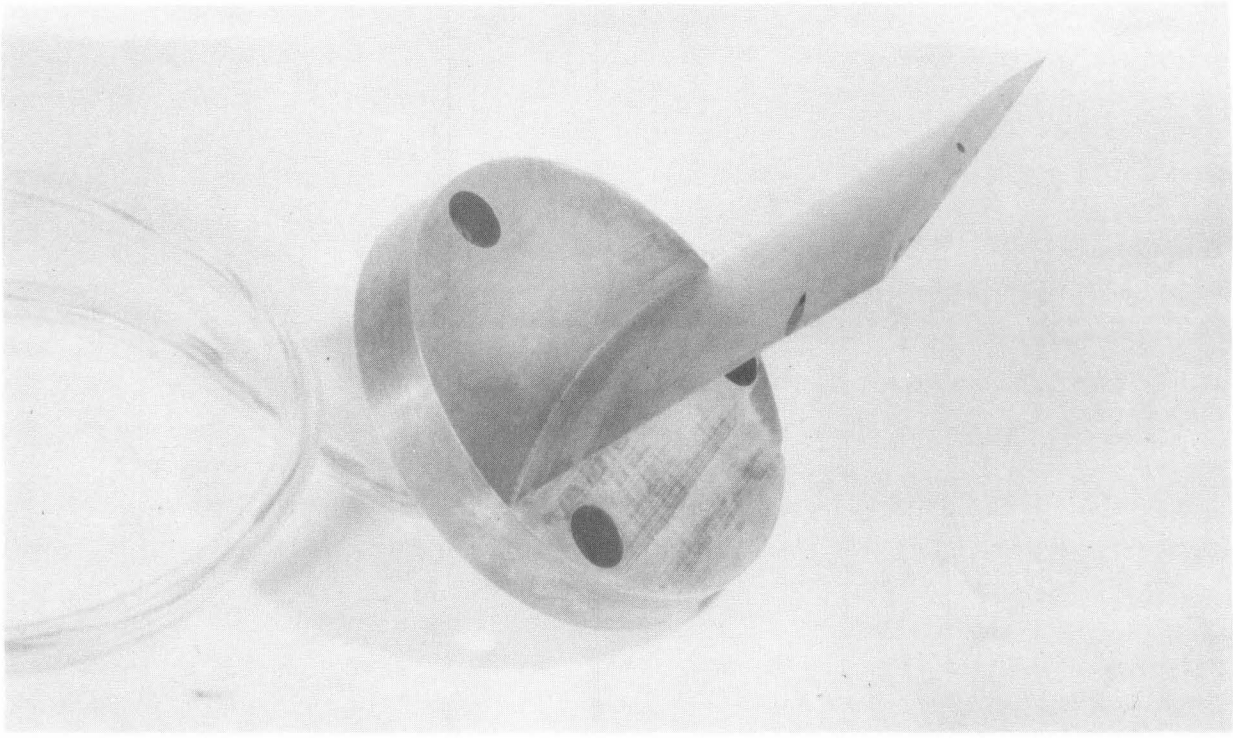

Figure 1(a) Model and base-plate.

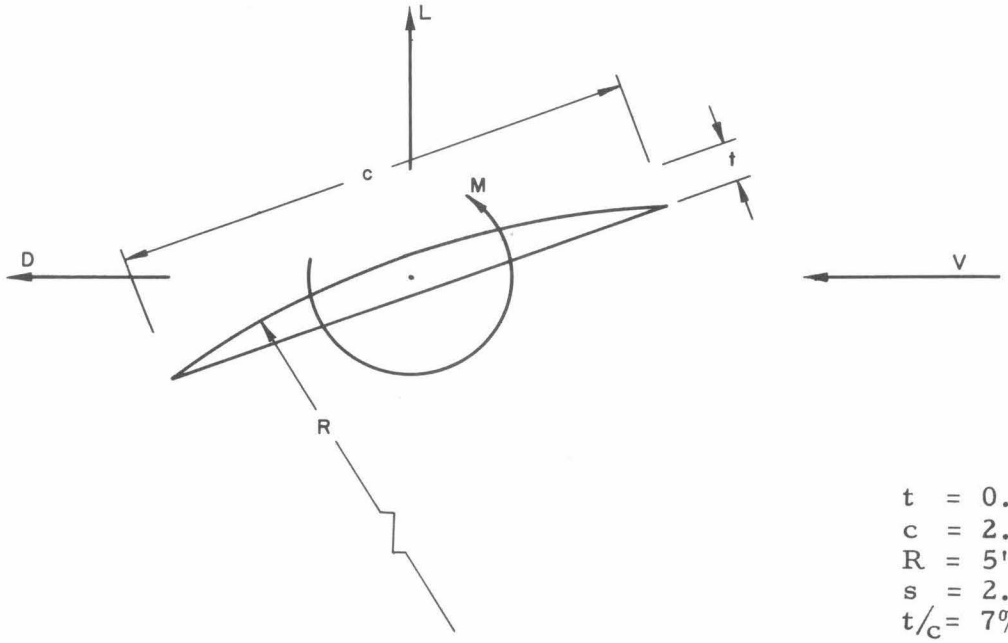

t = 0.19"
c = 2.77"
R = 5"
s = 2.85"
t/c = 7%

Figure 1(b) Dimensions of model and positive sense of forces and moments.

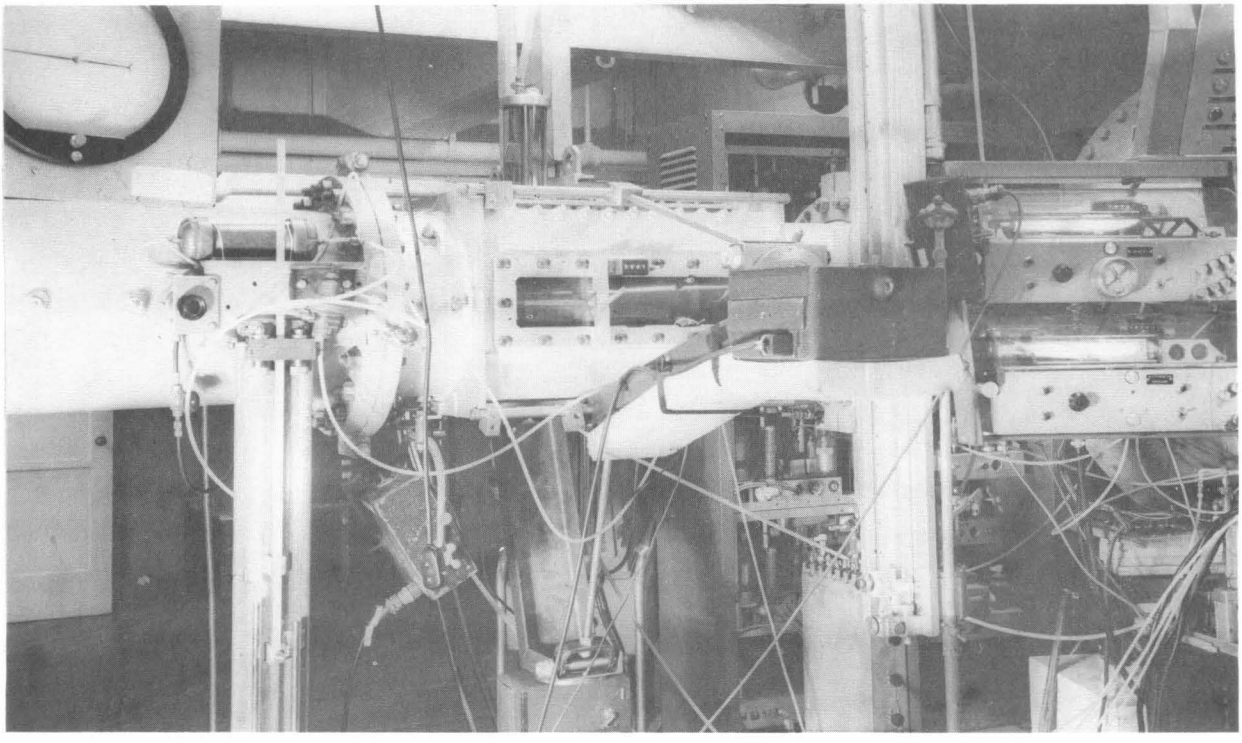

Figure 2 Test set-up showing working section with manometers and recording cameras.

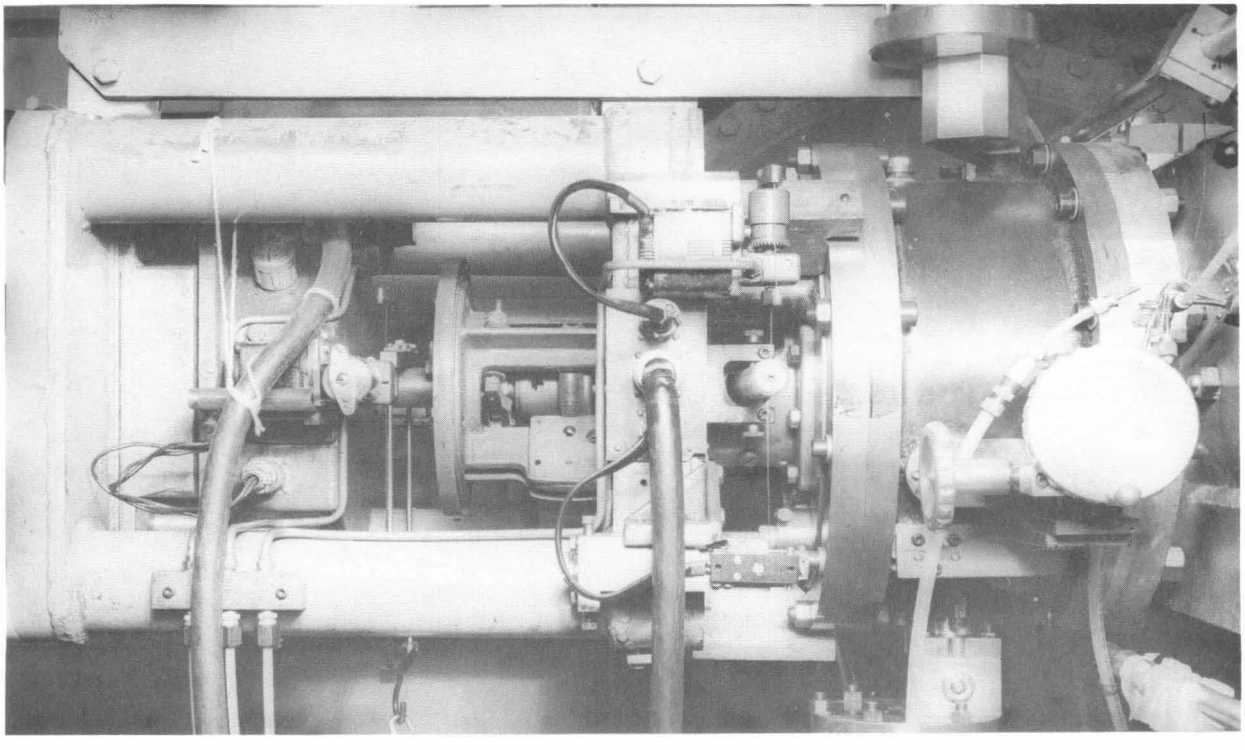

Figure 3 Close up of force balance mounted on tunnel (to right of picture).

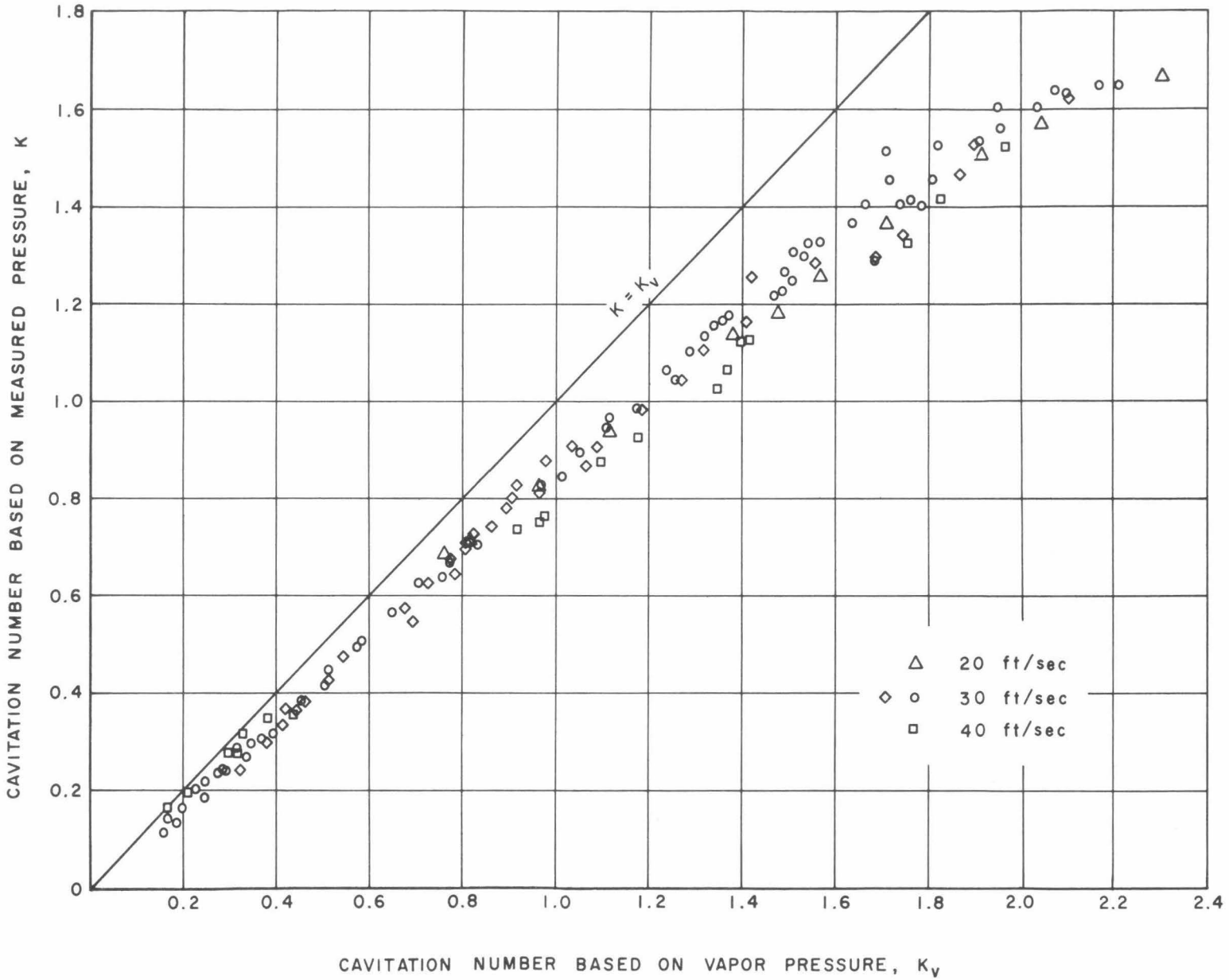

Figure 4 Comparison of measured cavitation number to that based on vapor pressure.

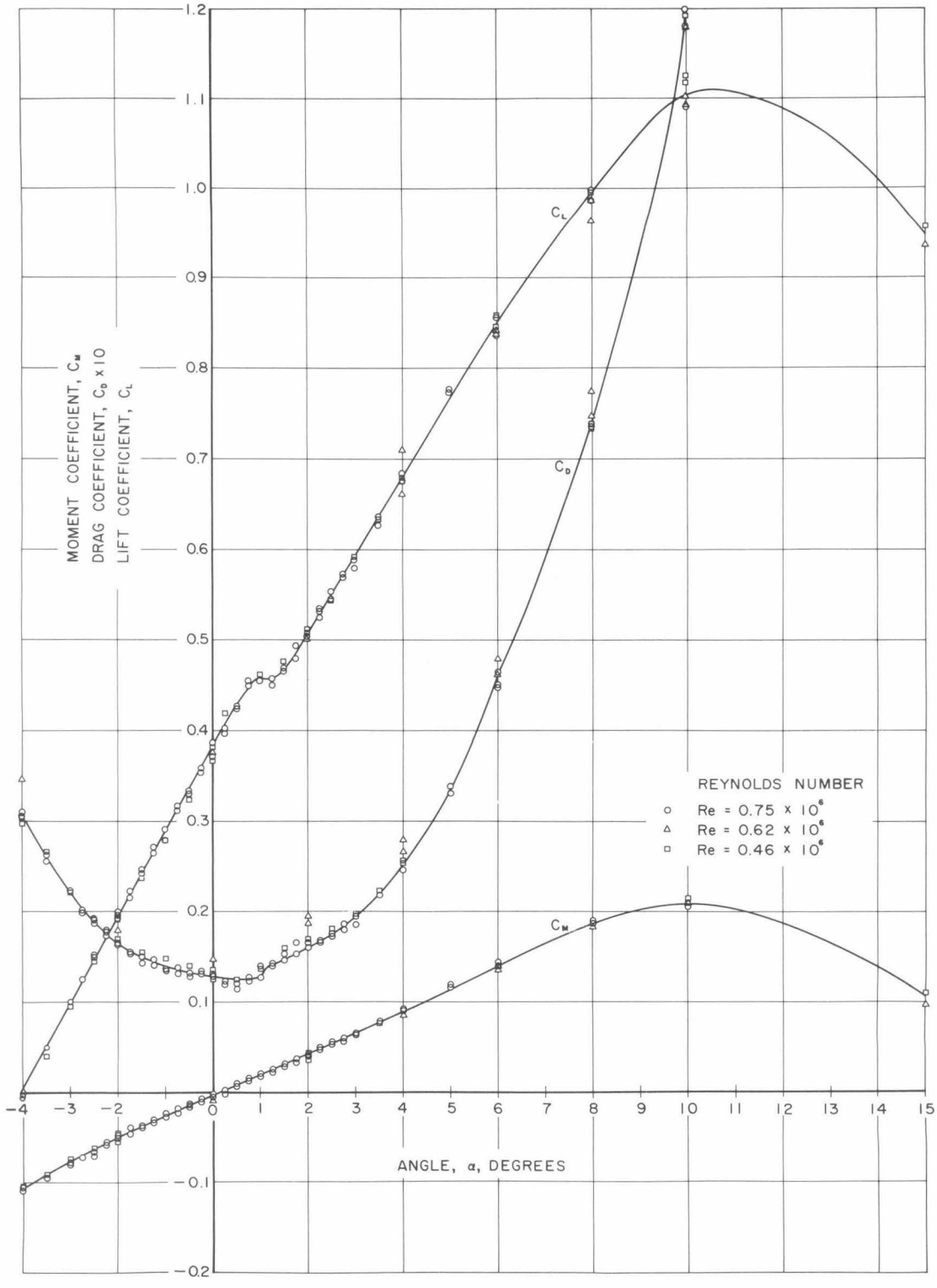

Figure 5 Force coefficients as functions of angle of attack for non-cavitating flow for several Reynolds numbers.

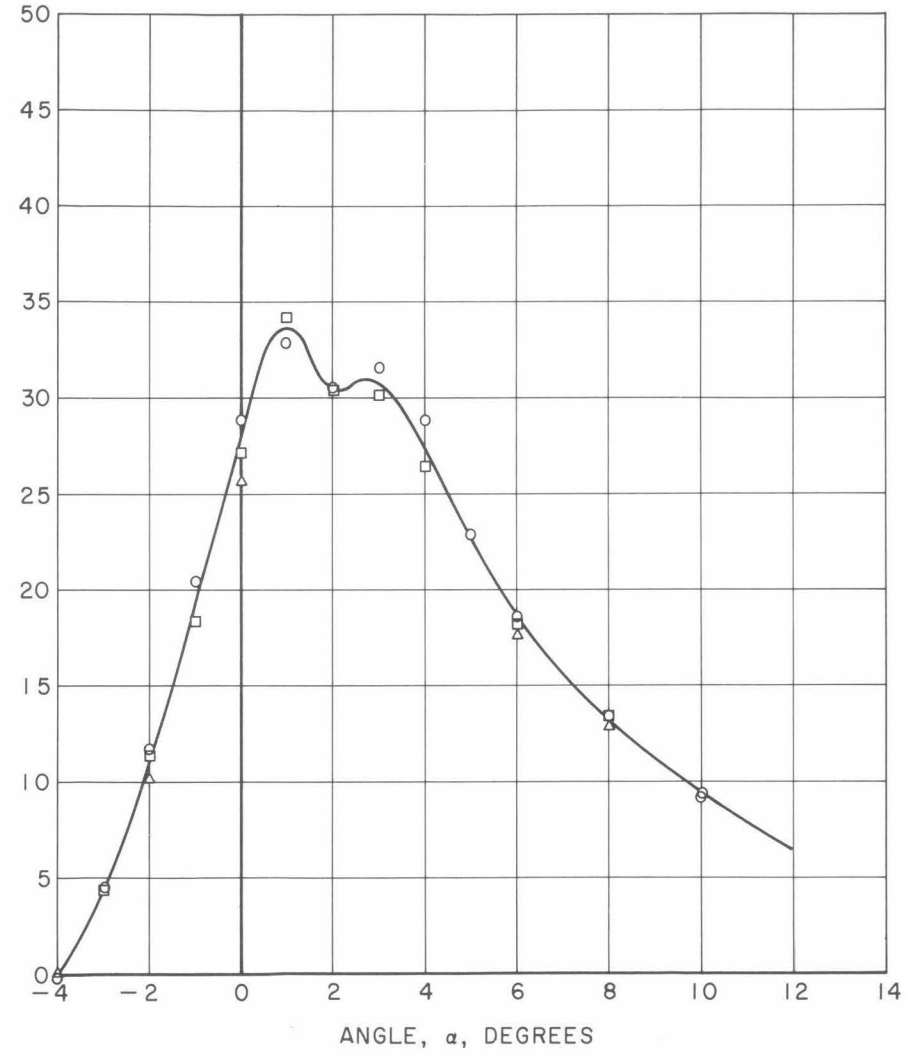

Figure 6 Lift to drag ratio as a function of angle of attack for non-cavitating flow.

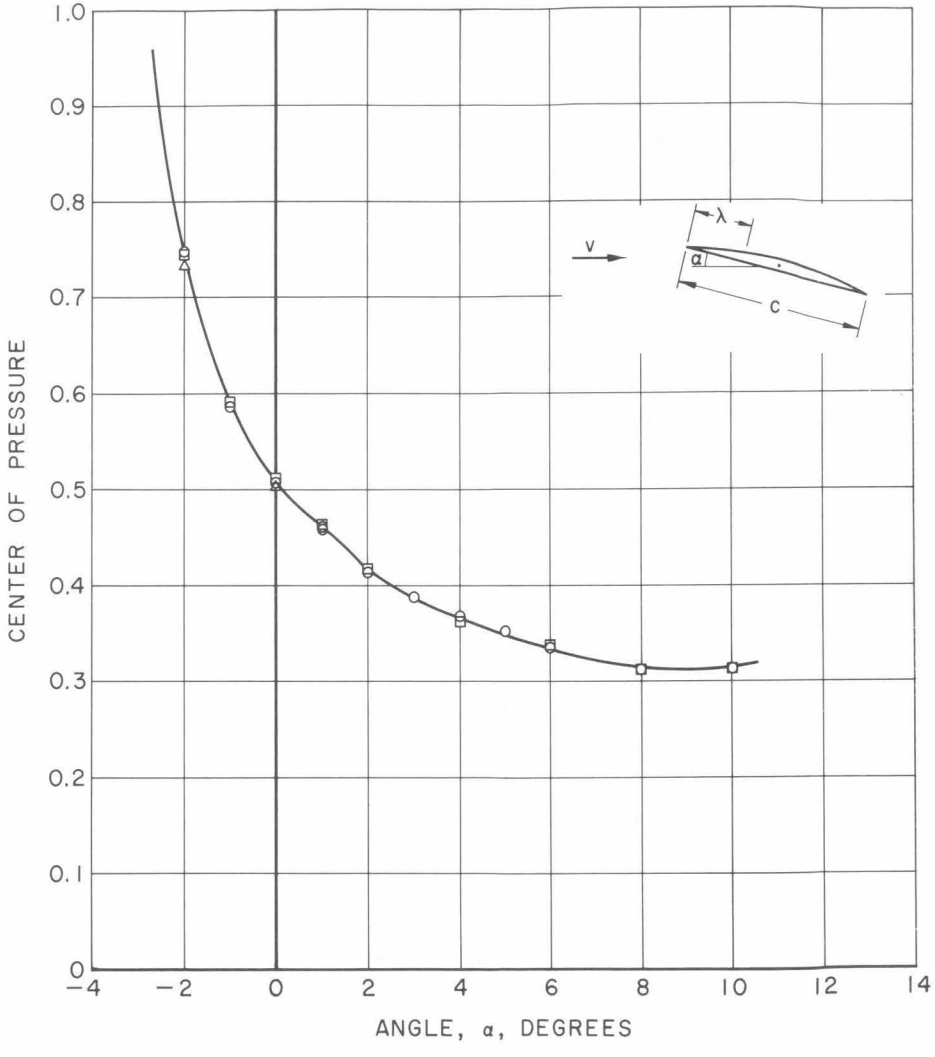

Figure 7 Centre of pressure variation with angle of attack for non-cavitating flow.

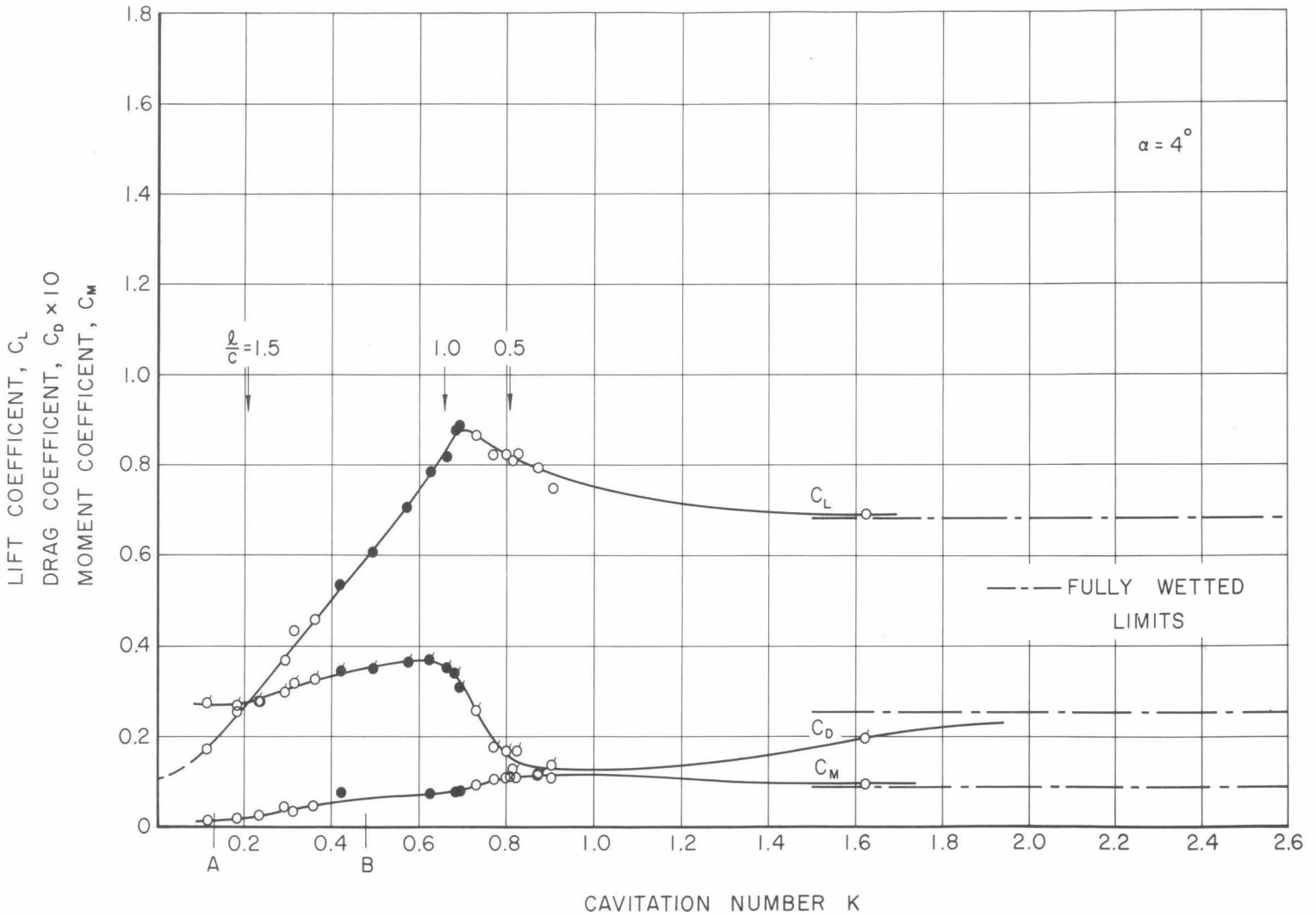

Figure 8(a) Force coefficients as functions of cavitation number for $\alpha = 4^\circ$.

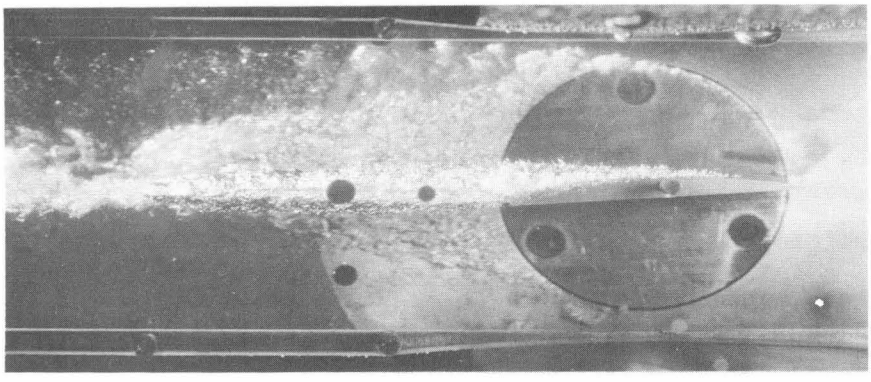

K = 0.131 A

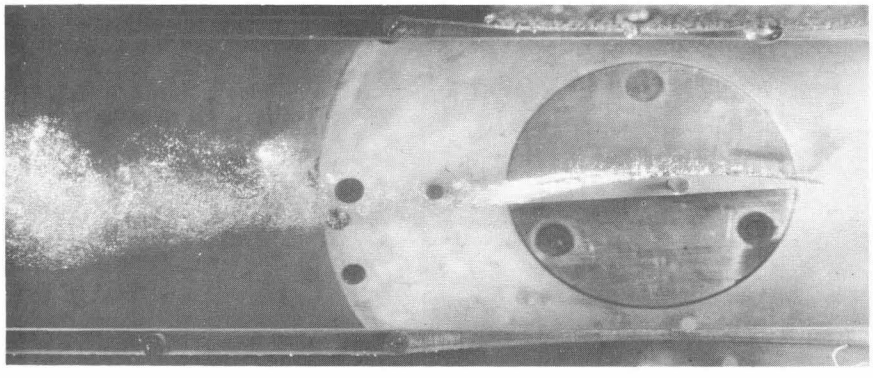

K = 0.480 B

Figure 8(b) Cavitation on model at $\alpha = 4^{\circ}$.

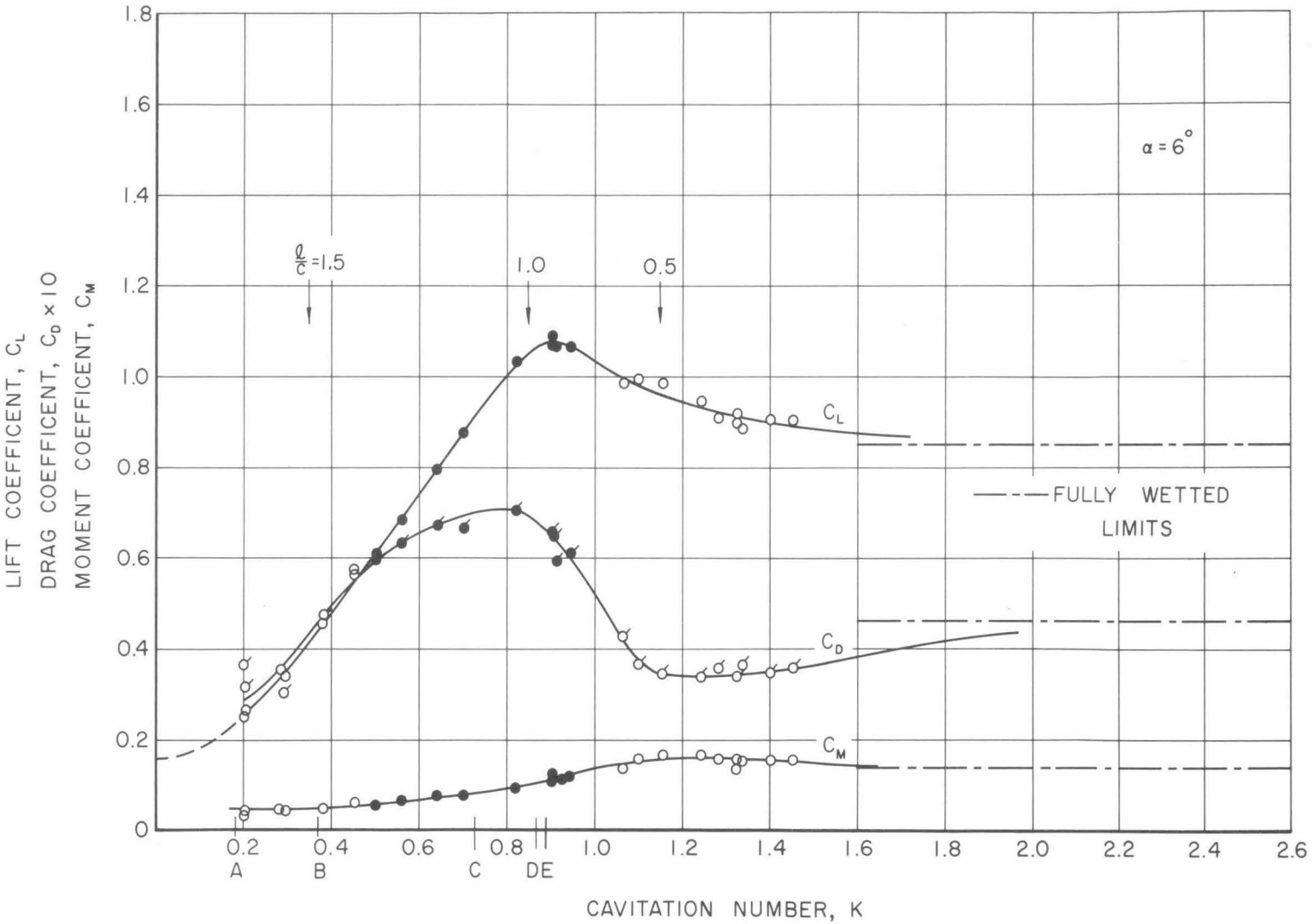

Figure 9(a) Force coefficients as functions of cavitation number for $\alpha = 6^\circ$.

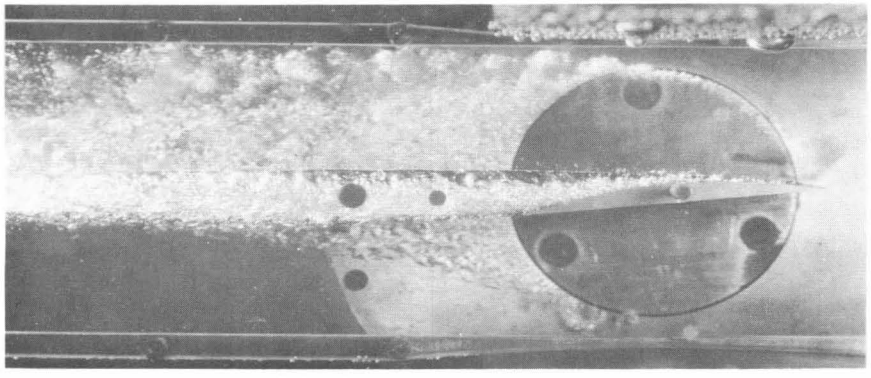

K = 0.183 A

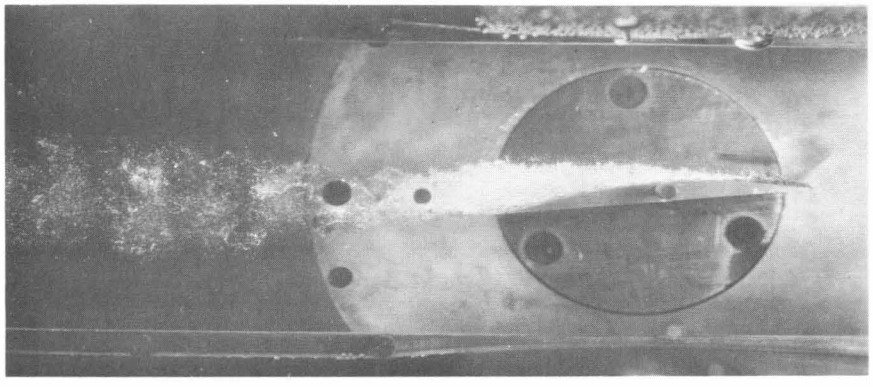

K = 0.386 B

Figure 9(b) Cavitation on model at $\alpha = 6^{\circ}$.

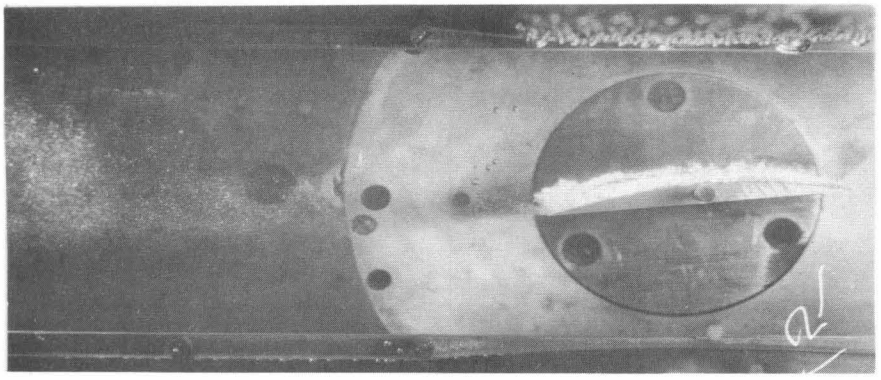

K = 0.730 C

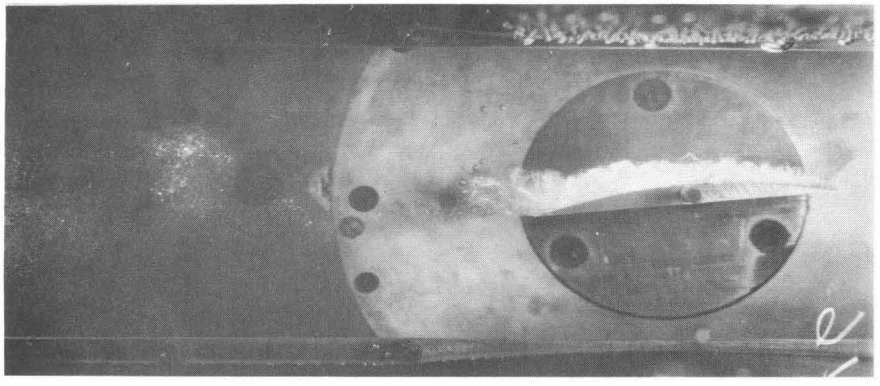

K = 0.870 D

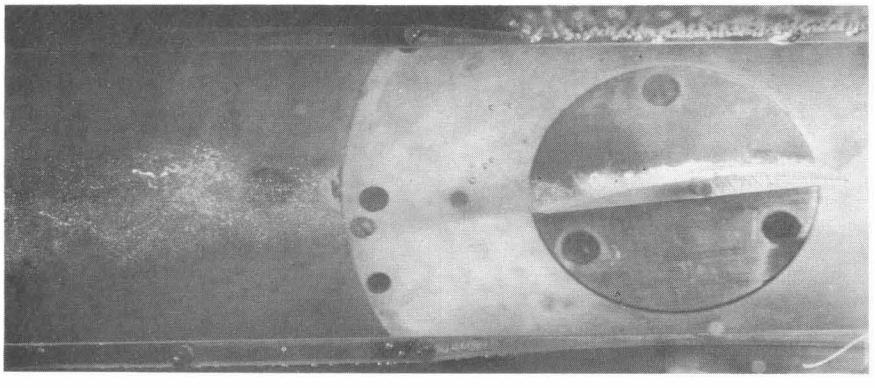

K = 0.890 E

Figure 9(b) Cavitation on model at $\alpha = 6^{\circ}$.

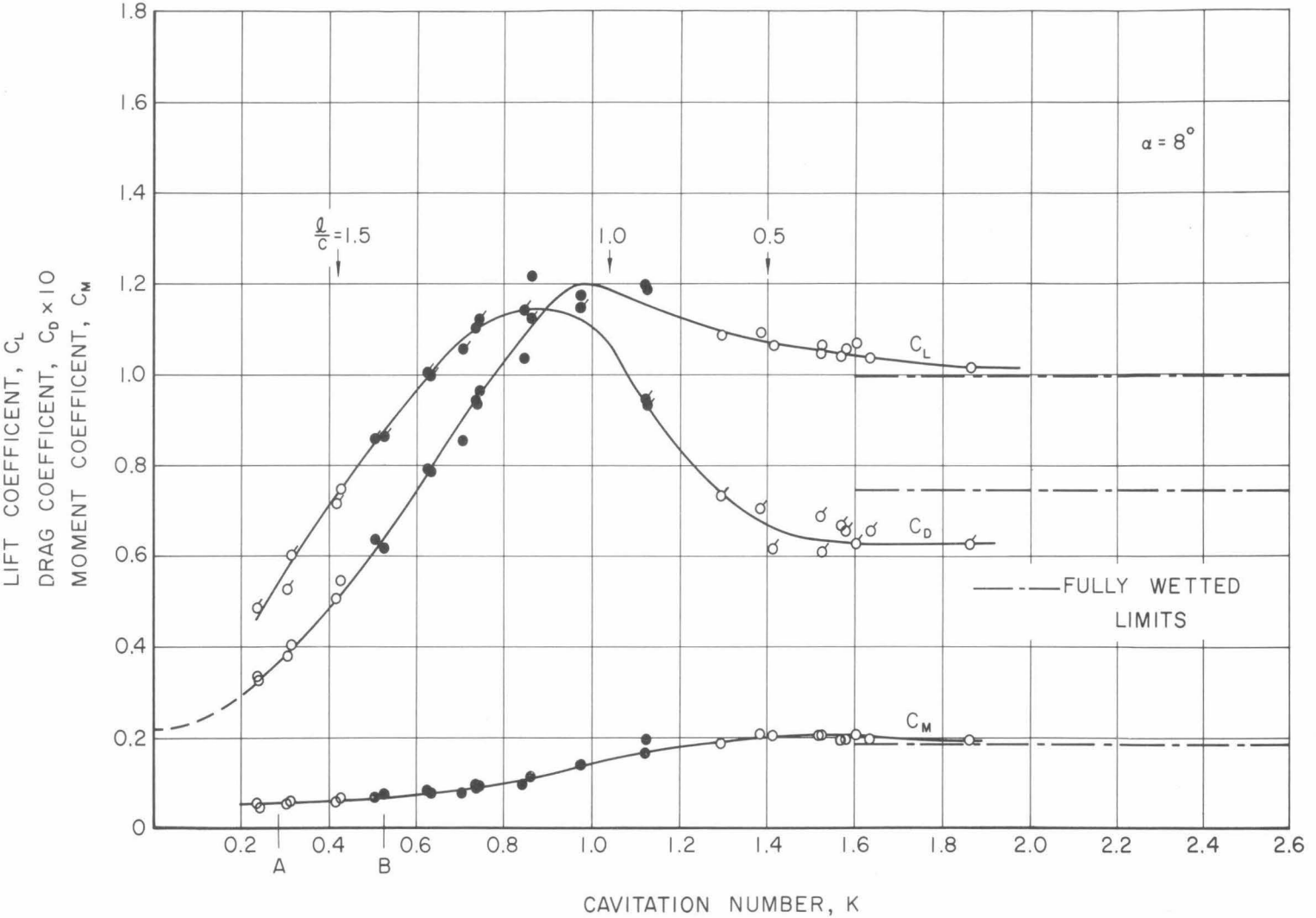

Figure 10(a) Force coefficients as functions of cavitation number for $\alpha = 8^{o}$.

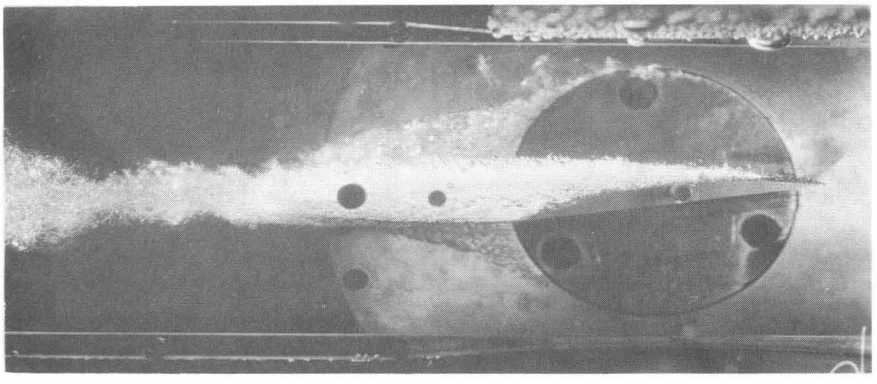

K = 0.285 A

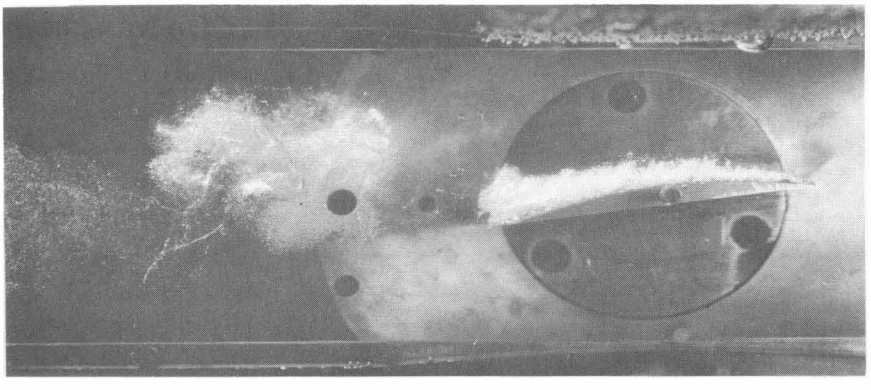

K = 0.522 B

Figure 10(b) Cavitation on model at $\alpha = 8^{\circ}$.

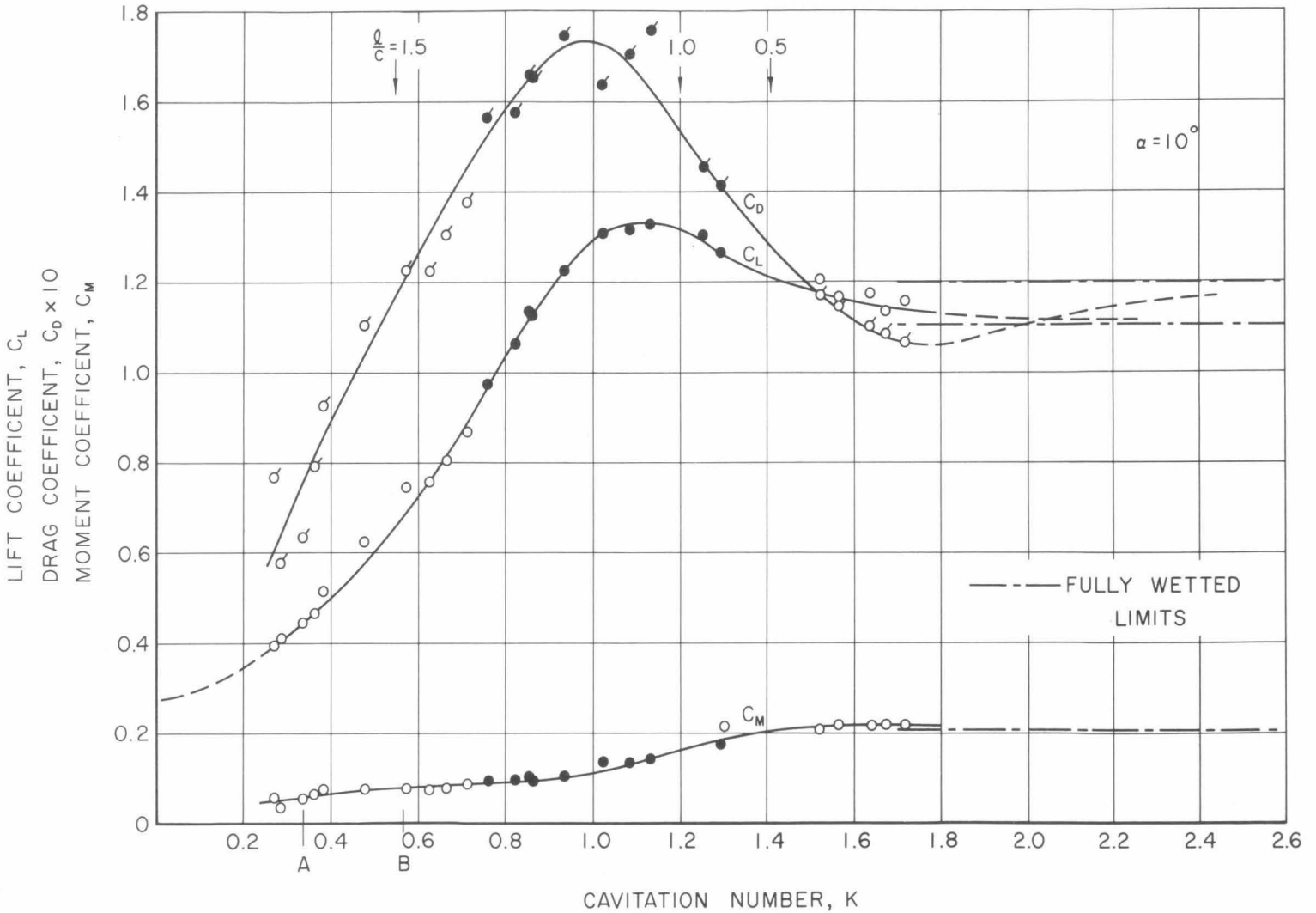

Figure 11(a) Force coefficients as functions of cavitation number for $\alpha = 10^\circ$.

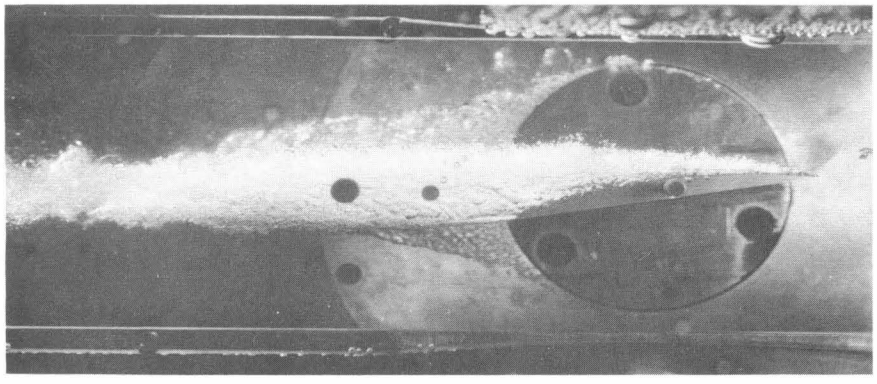

K = 0.331 A

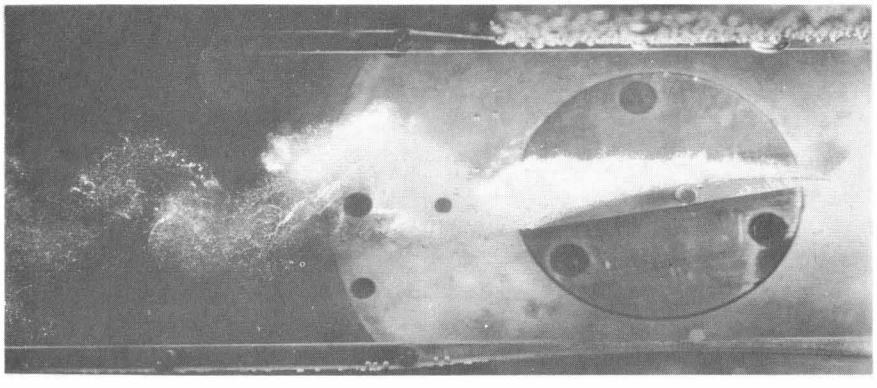

K = 0.561 B

Figure 11(b) Cavitation on model at $\alpha = 10^{\circ}$.

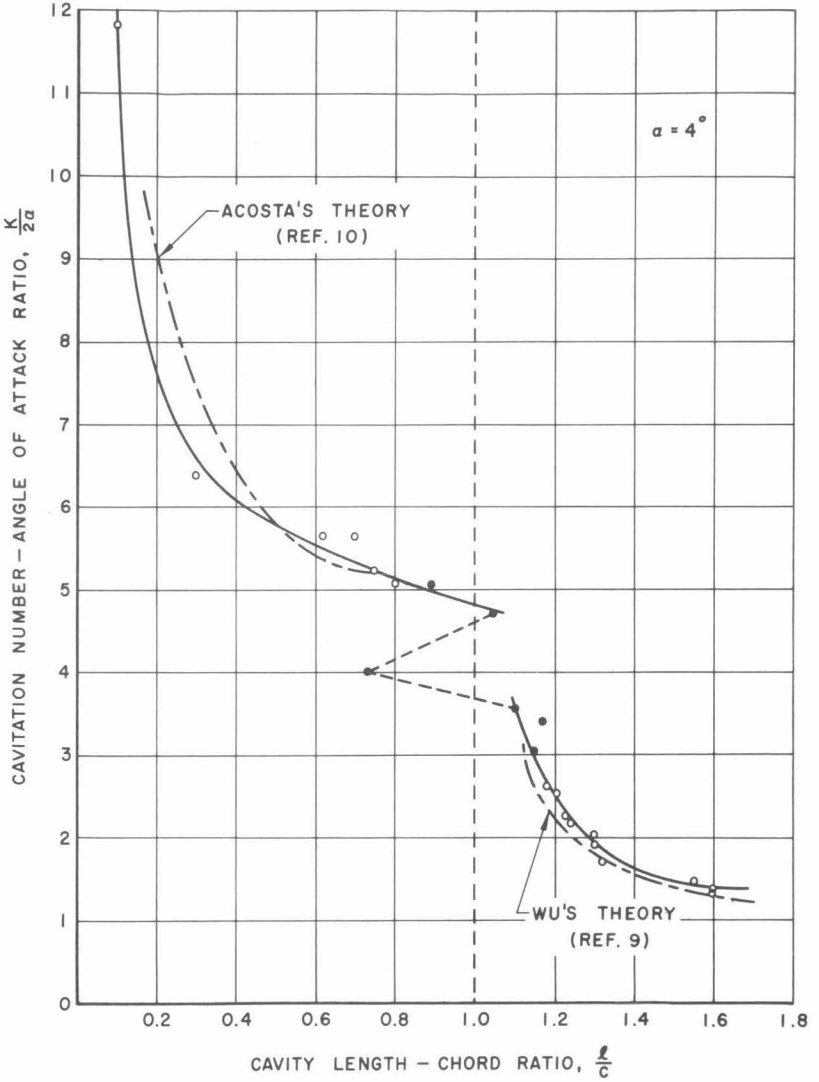

Figure 12 Cavitation number to attack angle ratio as a function of cavity length to chord ratio for $\alpha = 4^{o}$.

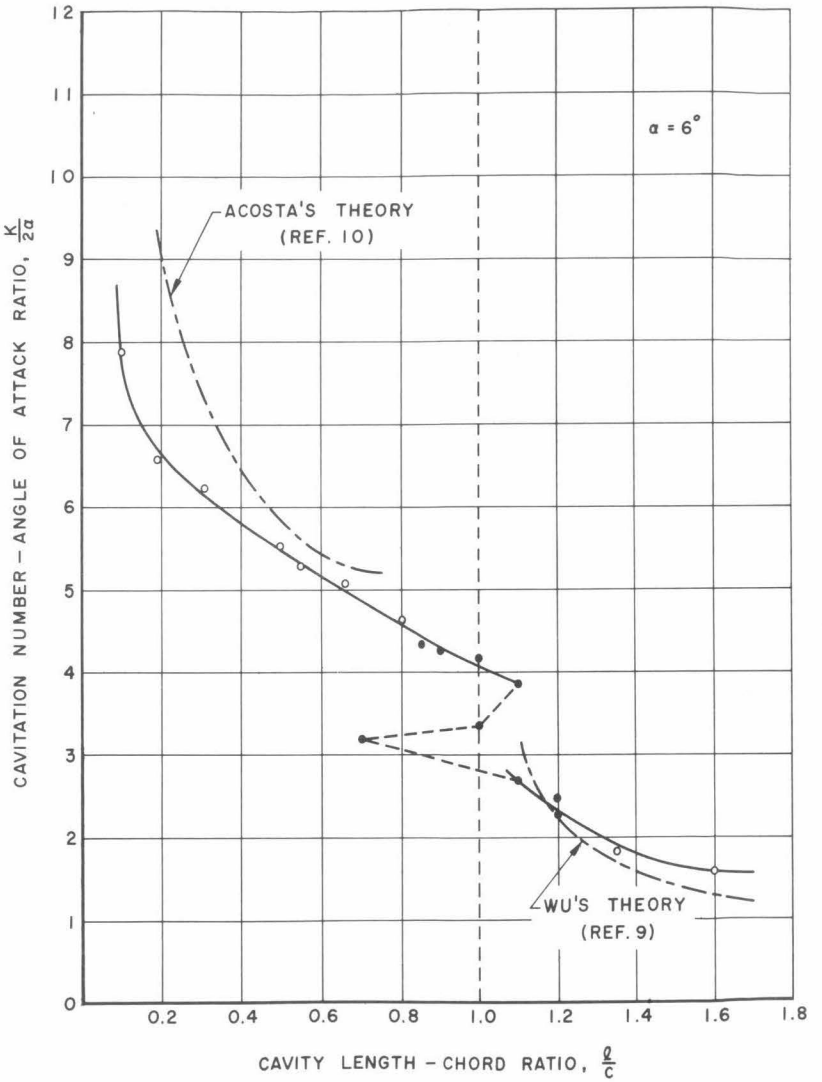

Figure 13 Cavitation number to attack angle ratio as a function of cavity length to chord ratio for $\alpha = 6^{o}$.

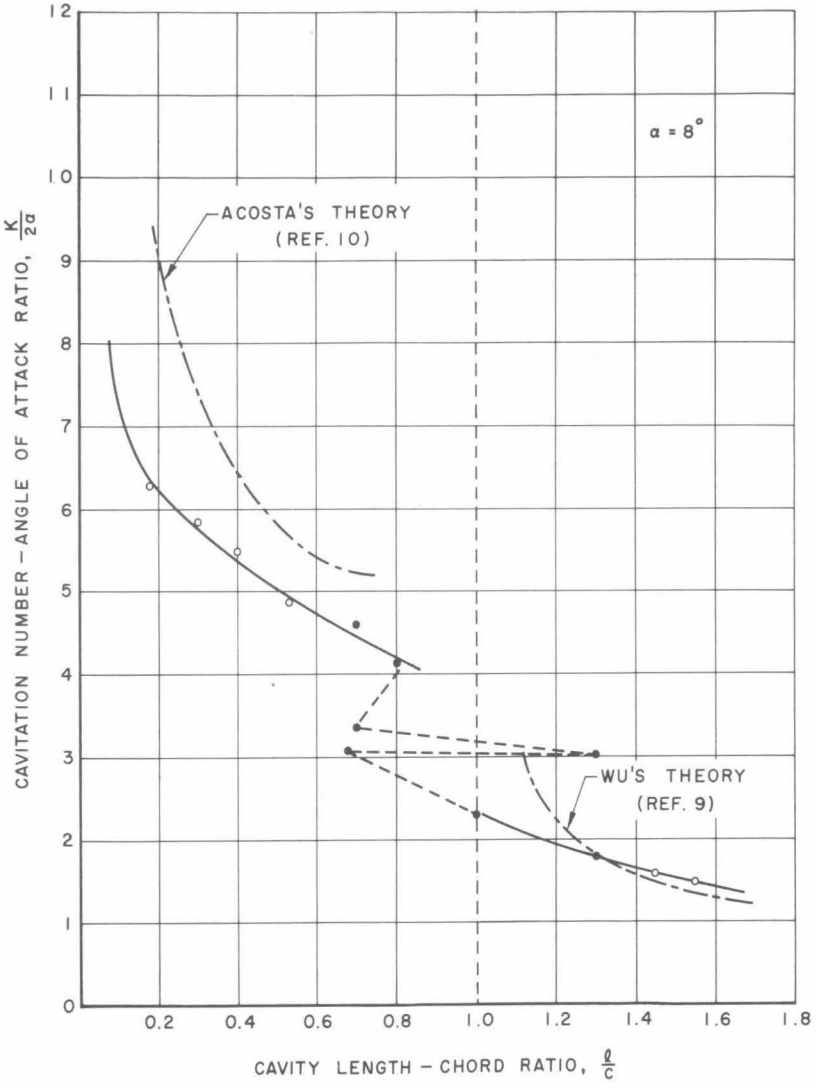

Figure 14 Cavitation number to attack angle ratio as a function of cavity length to chord ratio for $\alpha = 8^{o}$.

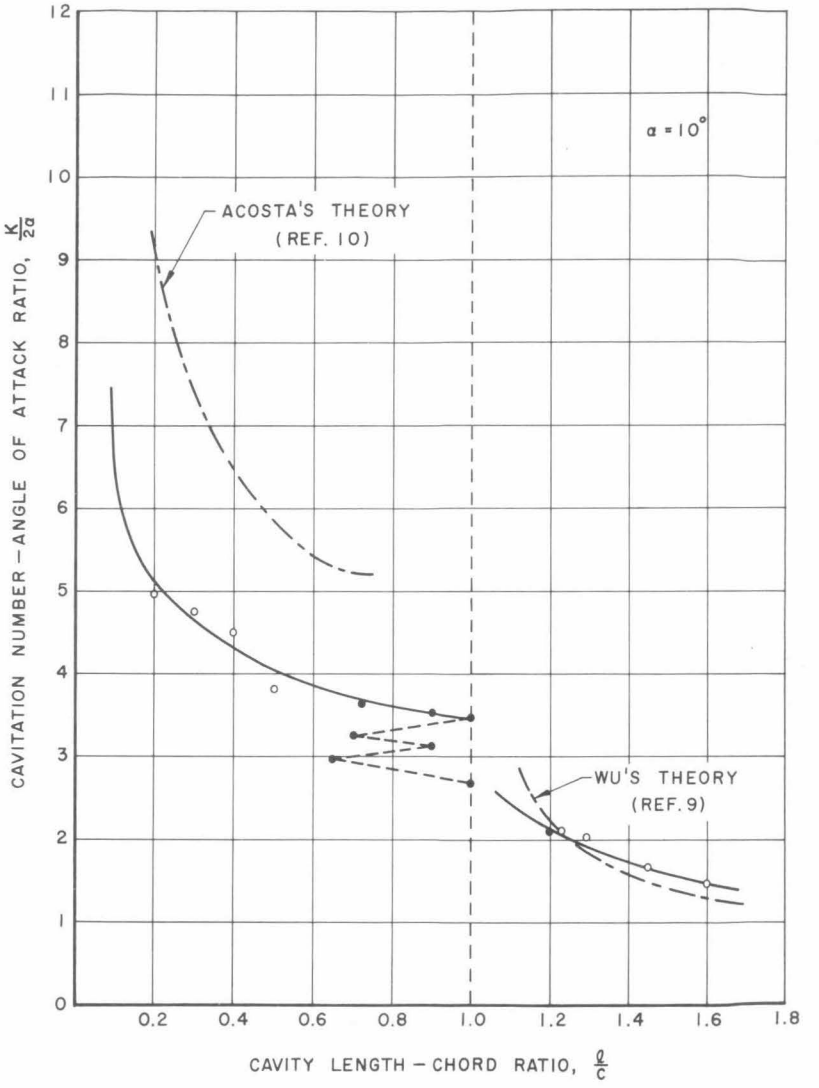

Figure 15 Cavitation number to attack angle ratio as a function of cavity length to chord ratio for $\alpha = 10^{o}$.

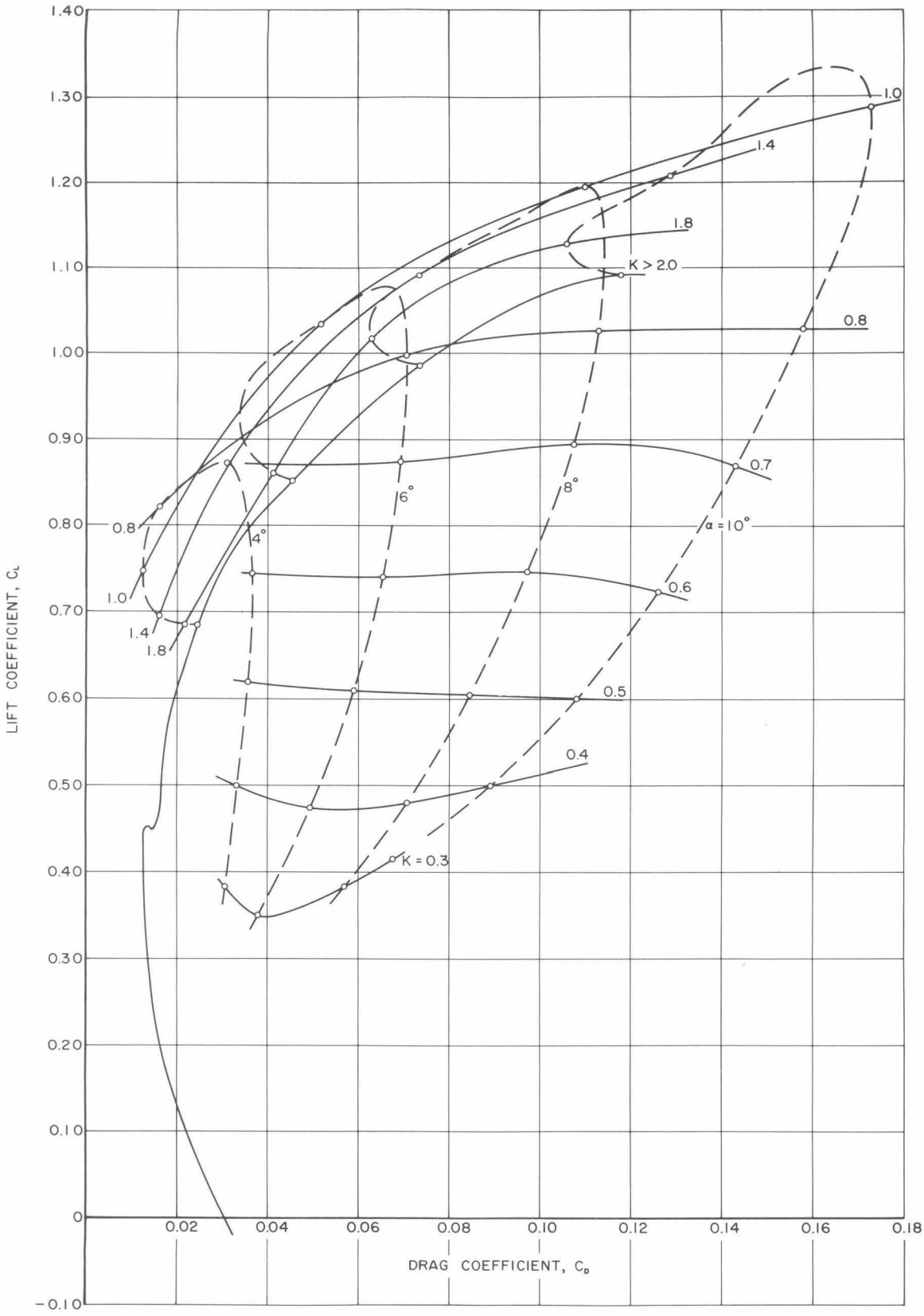

Figure 16 Polar diagram of the hydrofoil section for the range tested

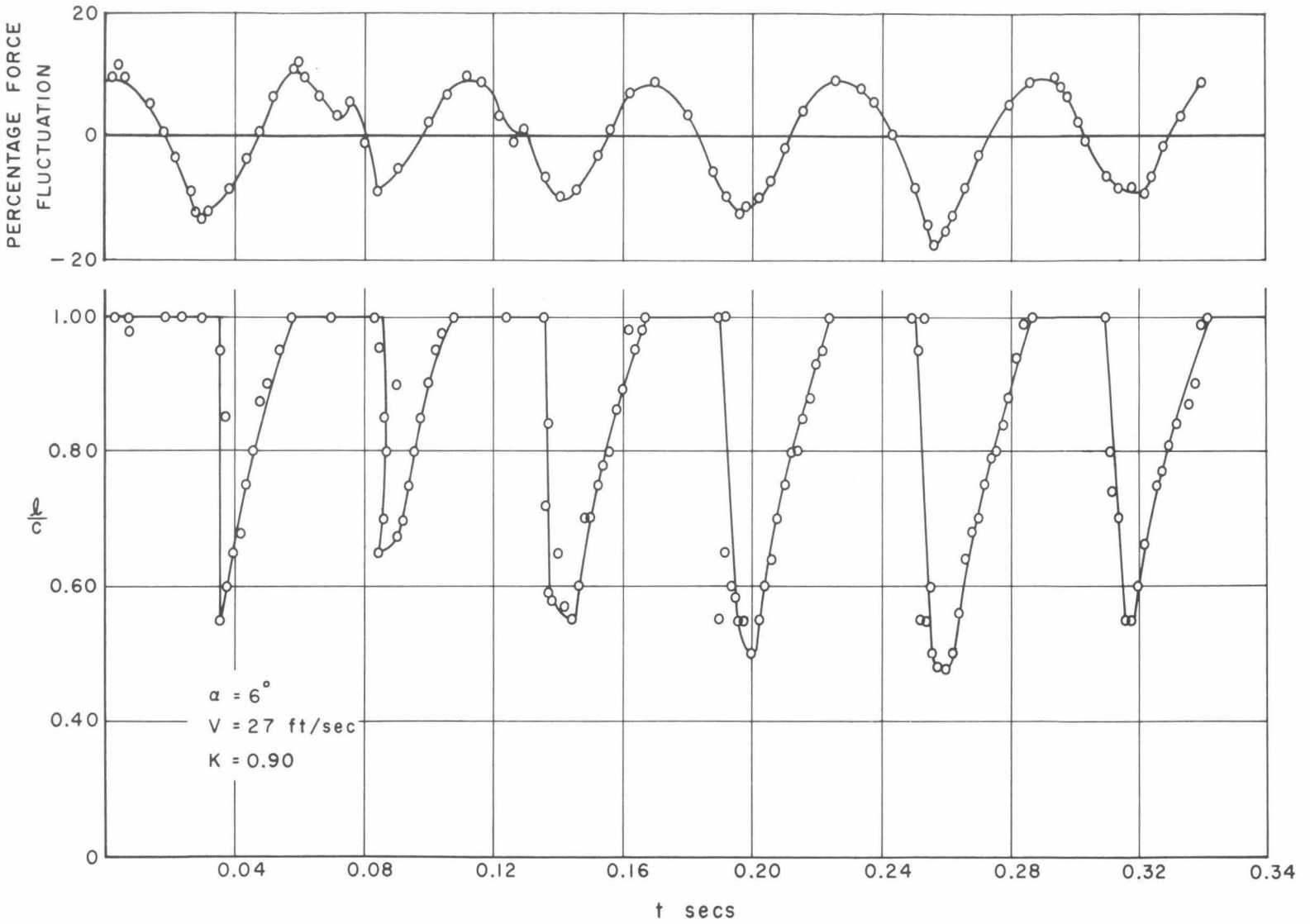

Figure 17 Percentage force fluctuations and cavity length to chord ratio as a function of the time in the region of maximum oscillations for $\alpha = 6^{\circ}$, V = 27 ft/sec and K = 0.90.

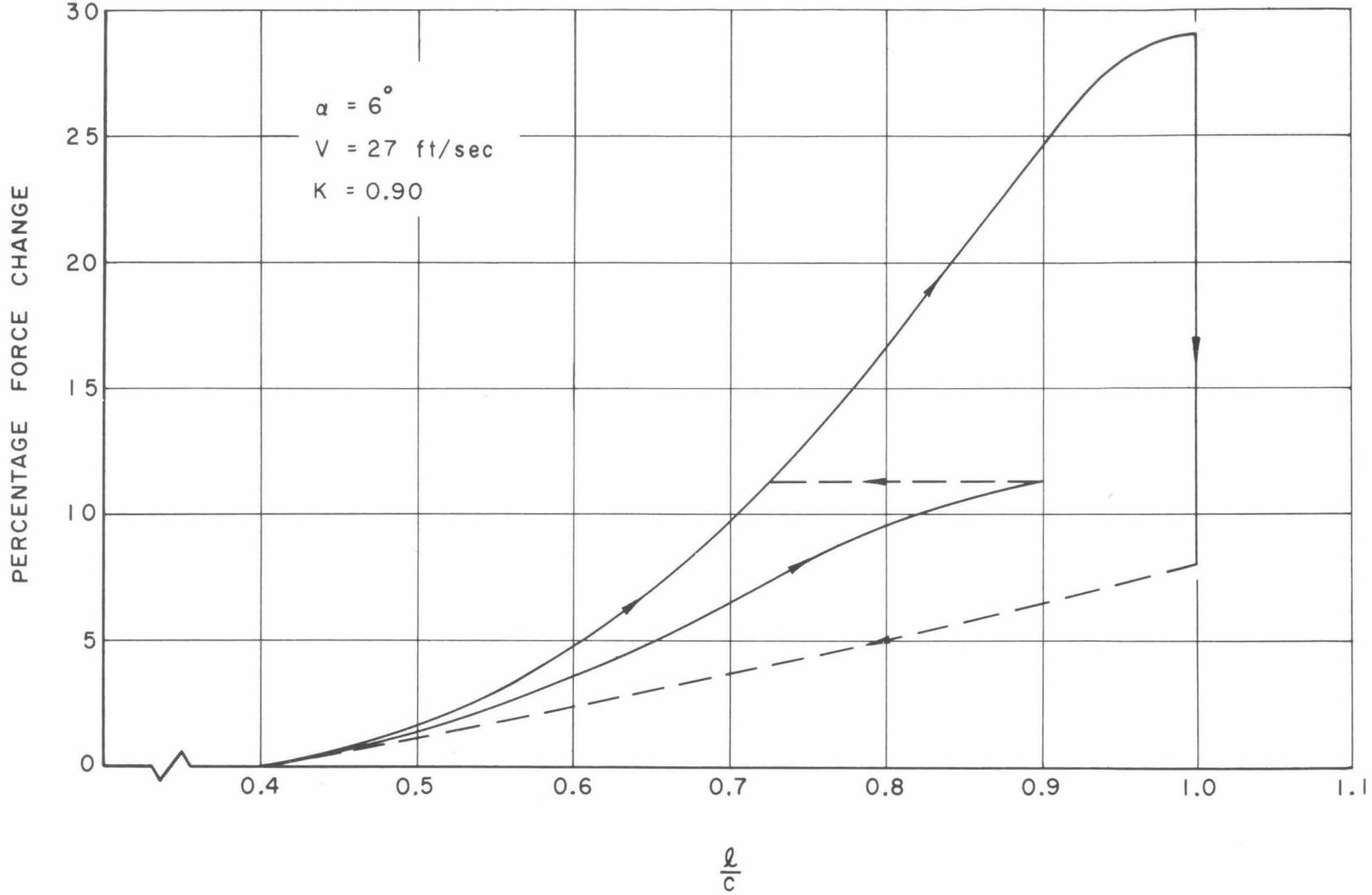

Figure 18 Percentage force change as a function of cavity length to chord ratio during maximum oscillations for $\alpha = 6^{\circ}$, V = 27 ft/sec and K = 0.90.

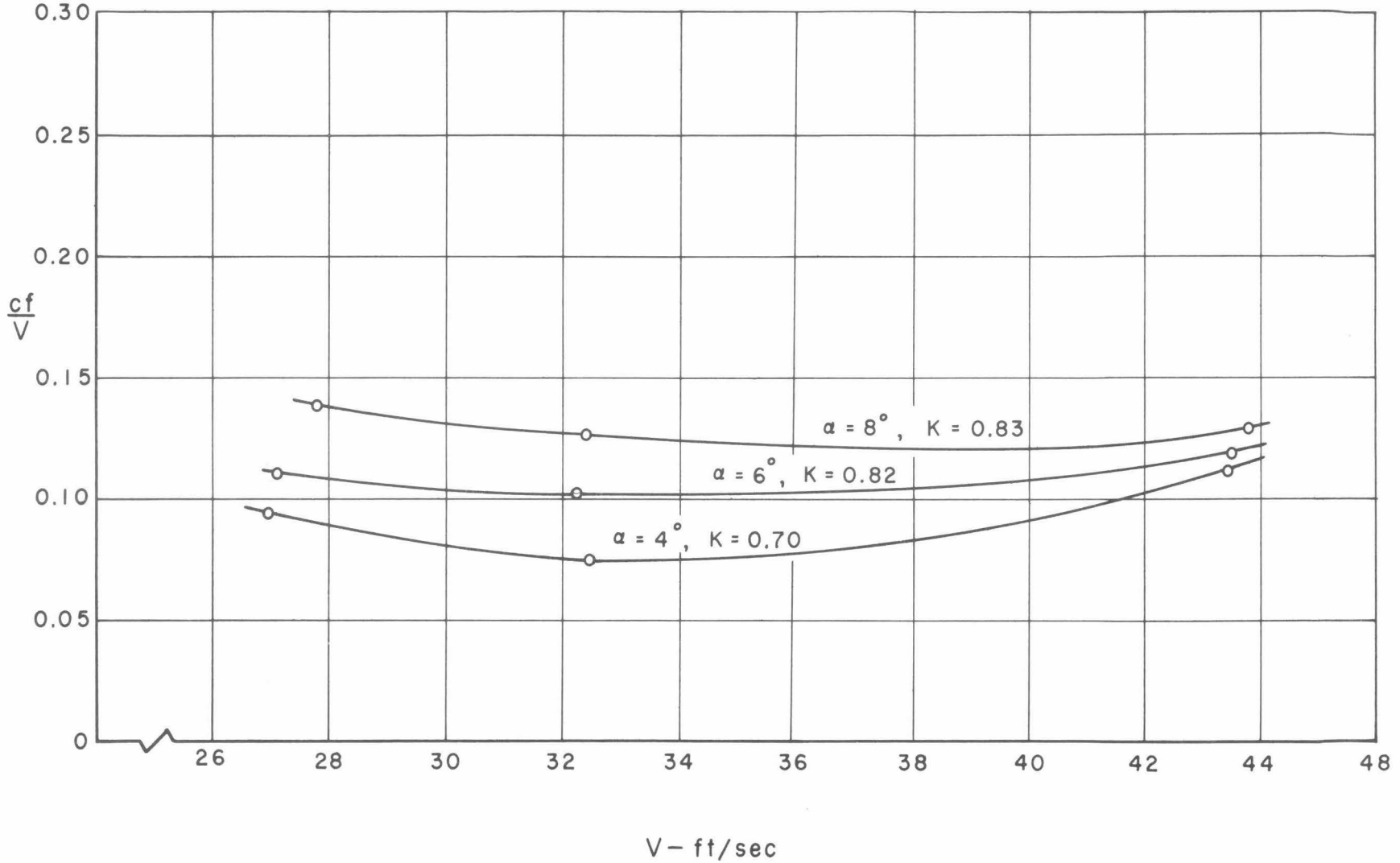

Figure 19 Reduced frequency during oscillations as a function of tunnel velocity.

IX. Appendices

Appendix 1

We present here the results of the tests carried out to determine the tare forces acting on the hydrofoil mounting disk. The results have been reduced to coefficient form to facilitate their application to the test data.

Figure A1.1 shows the lift force acting on the disk as a function of the cavitation number for different angles of attack. Figure A1.2 indicates the behavior of the drag force and Figure A1.3 illustrates the tare force corrections for lift, drag and moment in fully wetted flow, as a function of angle of attack.

The method for obtaining these results, as previously mentioned, is reported in Ref. 2.

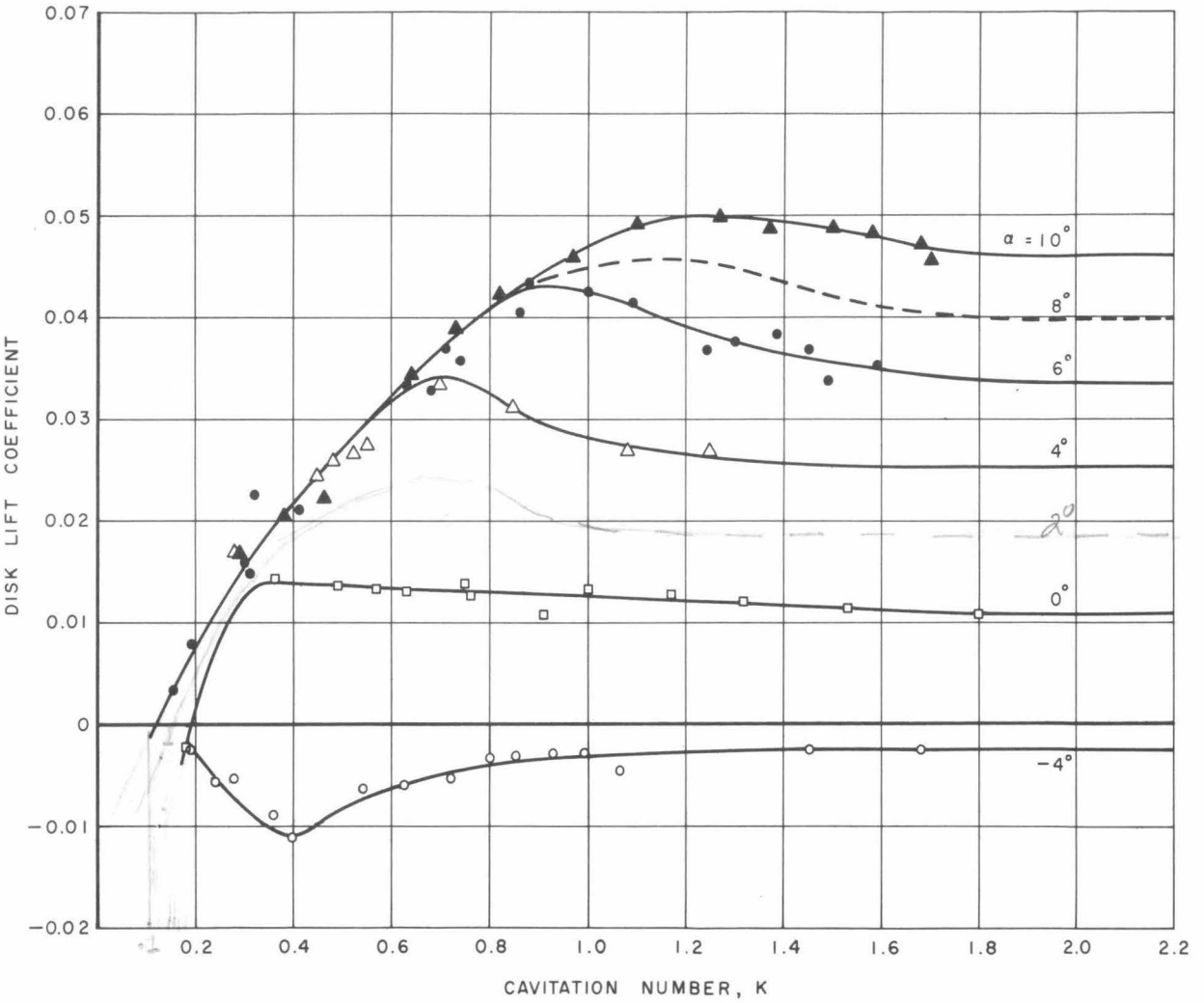

Figure A1.1 Tare lift force coefficient on mounting disk as a function of cavitation number.

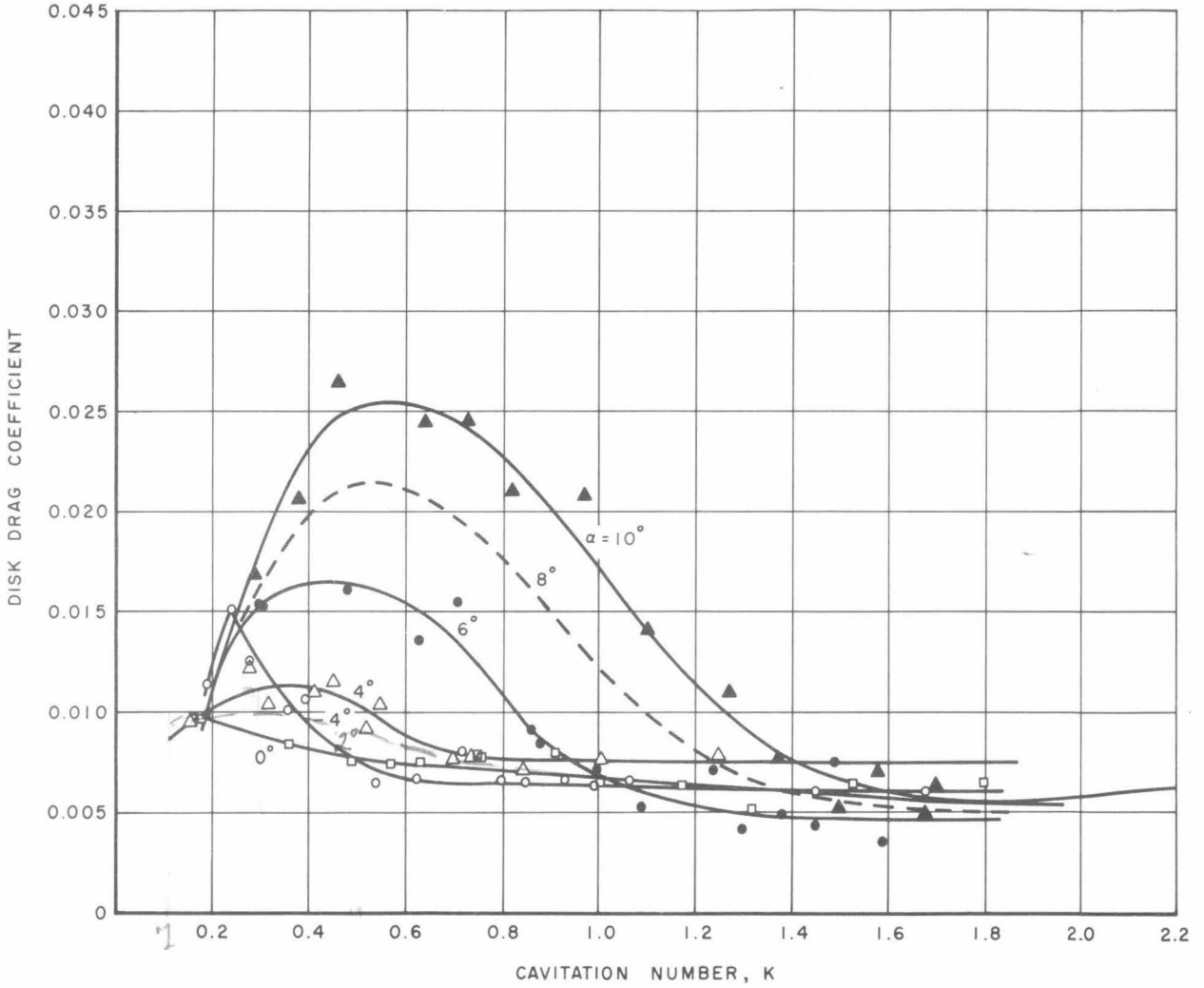

Figure A1.2 Tare drag force coefficient on mounting disk as a function of cavitation number.

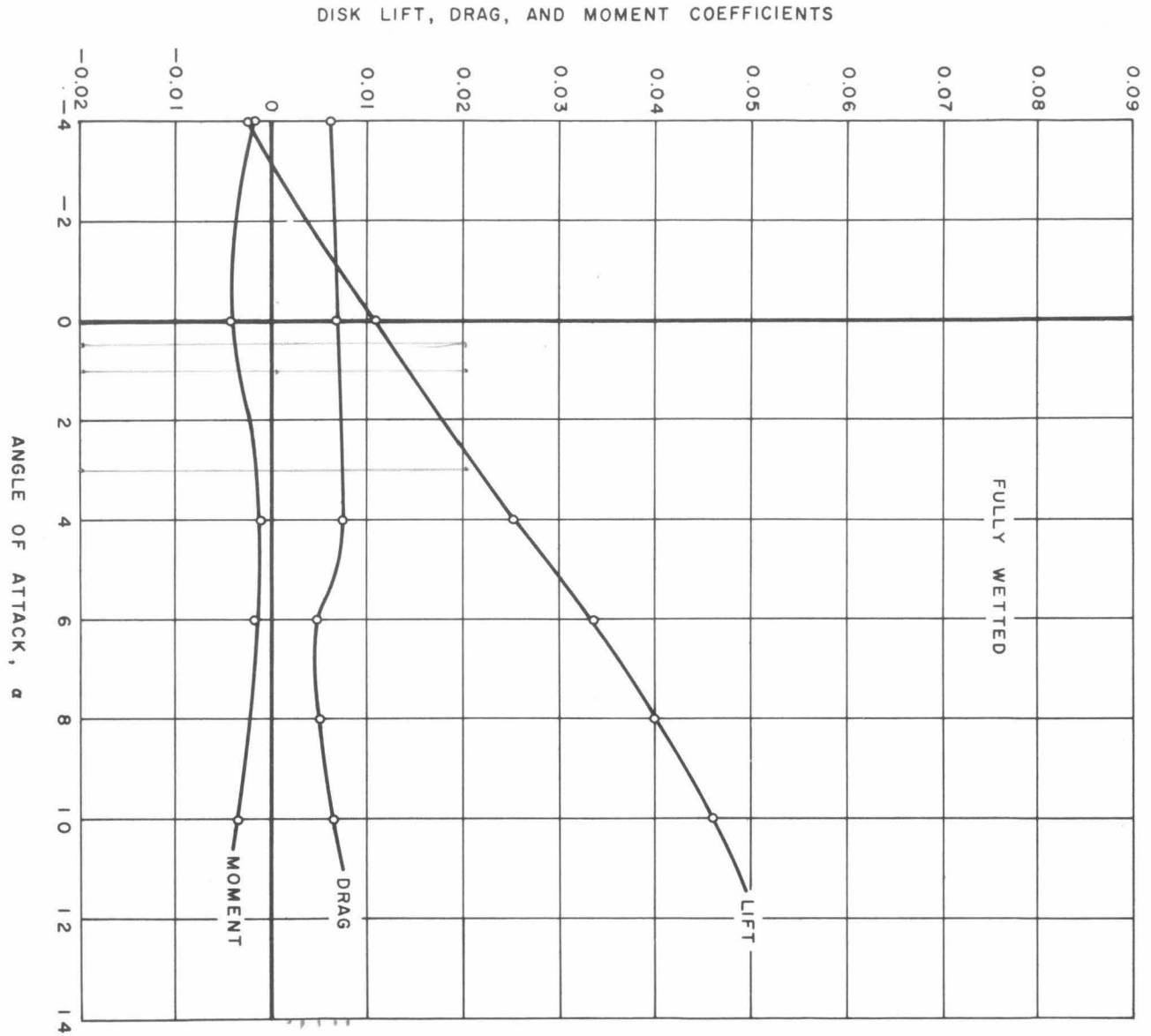

Figure A1.3 Tare force coefficients as a function of angle of attack for non-cavitating flow.

Appendix 2

The method of correcting for the model interference effects is presented in this appendix. Before proceeding with the method used it must be stated that this correction endeavors only to account for the induced circulation by the model and does not deal with other tunnel effects such as the wall effects and static pressure gradient effects. The notation to be used is illustrated in the following Figure.

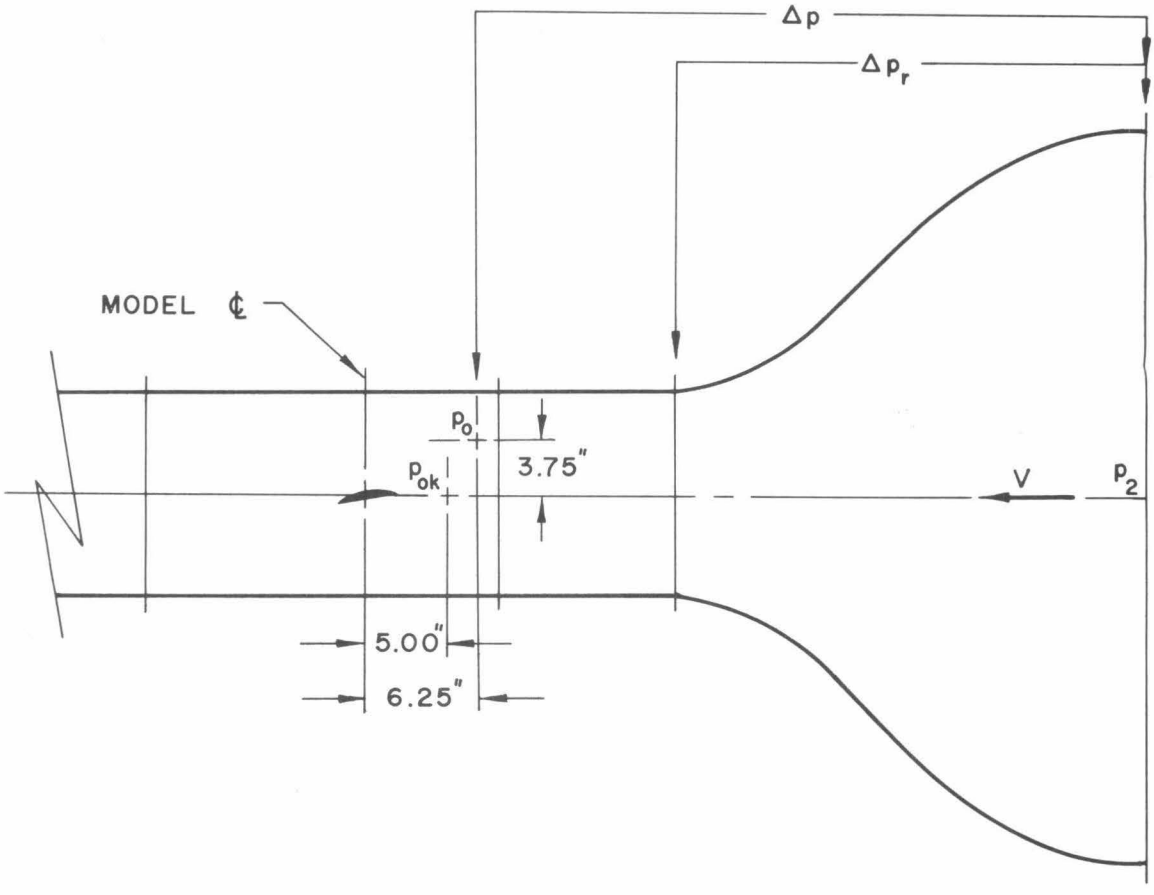

Figure A2.1 Diagrammatic sketch illustrating notation used in applying model interference corrections.

The method is designed so as to apply the corrections to the results in coefficient form. The procedure used is as follows: The static pressure was measured at all the pressure taps used in the working section (p_o, p_{ok}), as was the differential pressure used in calculating the dynamic head Δp, for the entire range of velocities used in the experiment.

All conditions of cavitation on the model at various angles of attack were considered. The differential pressure across the main nozzle Δp_r was recorded and this reading used as a reference, it being relatively insensitive to the circulation effect. The lift force on the model was recorded this being a measure of the induced circulation around the hydrofoil.

The ratio

$$\frac{p_2 - p_o}{\Delta p_r} = \frac{\Delta p}{\Delta p_r} ,$$

is then plotted as a function of C_L^*, the lift coefficient based on the uncorrected dynamic head Δp. This ratio is a function of C_L, say $h(C_L)$. The value of this function at zero lift is defined as

$$h(0) = \frac{p_2 - p}{\Delta p_r} \qquad (1)$$

where we now define p as the true working section static pressure. From these results the following correction procedure can be evolved. From equation (1) we get that

$$\frac{p - p_o}{\Delta p} = \frac{p_2 - h(0)\Delta p_r - p_o}{\Delta p}$$

$$= \frac{h(C_L) - h(0)}{h(C_L)} = f(C_L), \text{ say}$$

hence $$p = f(C_L)\,\Delta p + p_o$$

The force coefficients obtained directly from the experiment are defined as (in suitable units)

$$C_f^* = \frac{F}{(p_2 - p_o)} = \frac{F}{\Delta p}$$

The corrected force coefficient, however, is

$$C_f = \frac{F}{(p_2 - p)}$$

hence, we get

$$C_f = \frac{F}{p_2 - f(C_L)\Delta p - p_o} ,$$

$$= \frac{F}{\Delta p[\,1 - f(C_L)]} ,$$

i.e. $$C_f = \frac{C_f^*}{1 - f(C_L)} . \qquad (2)$$

Hence the corrected force coefficient may be obtained from the force coefficient obtained from direct measurement, once the function $f(C_L)$ has been obtained.

In a similar way, the cavitation number can be corrected. Since the measured cavitation number is

$$K^* = \frac{p_{ok} - p_k}{\Delta p} ,$$

the corrected cavitation number is

$$K = \frac{(p - p_k)}{(p_2 - p)} ,$$

$$= \frac{f(C_L)\Delta p + p_o - p_k}{p_2 - f(C_L)\Delta p - p_o} ,$$

$$= \frac{f(C_L)\Delta p + p_{ok} - p_k - p_{ok} + p_o}{\Delta p[1 - f(C_L)]} ,$$

$$= \frac{f(C_L)}{1 - f(C_L)} + \frac{K^*}{1 - f(C_L)} - \frac{\delta p_k}{\Delta p[1 - f(C_L)]} ,$$

$$K = \frac{1}{1 - f(C_L)} \left(K^* + \left[f(C_L) - \frac{\delta p_k}{\Delta p} \right] \right) \quad (3) .$$

All the functions in equations (2) and (3) can be obtained from the calibration tests, hence the corrected force coefficients and cavitation numbers can be found.

The functions

$$\frac{1}{1 - f(C_L)} \quad \text{and} \quad \left[f(C_L) - \frac{\delta p_k}{\Delta p} \right]$$

are shown plotted in Figure A2.2.

The results show quite a large scatter particularly in the latter function. This is due to the fact that the pressure differences

δp_k being measured are quite small and due to the normal surging in the pressure lines to the manometers this difference is extremely difficult to obtain with accuracy, thus giving rise to the large scatter. This effect is also apparent in the graph for the function $1/[1 - f(C_L)]$ although here the effect is relatively much smaller and a definite trend in the correction with lift coefficient is evident. At a lift coefficient of 1.0 this correction is approximately 3 percent.

The corrections have been presented as functions of lift only. This is not to say that there is no drag effect on the measurements. A drag effect was looked for in the results but this, it is felt, was lost in the scatter as the drag effect at the angles of attack investigated are of the same order of magnitude as the scatter obtained.

It seems, therefore, that short of improving the accuracy of the normal measuring techniques the drag effect is unobtainable at these low angles of attack. However, at larger angles of attack, of the order of 25°, this effect should be apparent.

The points shown plotted, as mentioned, cover all the experimental conditions investigated. However, no endeavor is made to distinguish these points as no definite dependence was observed on velocity, static pressure, etc.

It would seem, at first glance that no correction would be necessary to the data at zero lift. This is indeed the case for the factor $1/[1 - f(C_L)]$ which is unity at zero lift. The factor

$[f(C_L) - \frac{\delta p_k}{\Delta p}]$, however, incorporates in it a correction which accounts for the use of two different pressure taps p_{ok} and p_o in the working section for the determination of the cavitation number. At zero lift we see that, since f(O) is zero, $-\delta p_k/\Delta p$ has the value 0.02, approximately.

$$\text{i.e.} \qquad \frac{p_o - p_{ok}}{\Delta p} \simeq 0.02$$

This pressure difference arises from the boundary layer effect and its value, in fact, checks with calibration results of the two-dimensional working section obtained in Ref. 2.

The corrections were applied to the results in the following manner. The force coefficients and cavitation number are calculated from the experimental readings. For each data point the corrections $1/[1 - f(C_L)]$ and $[f(C_L) - \frac{\delta p_k}{\Delta p}]$ for the given lift is read off Figure A2.2 and applied to the results. The tare force correction is then applied and these final results are the ones shown plotted in the report.

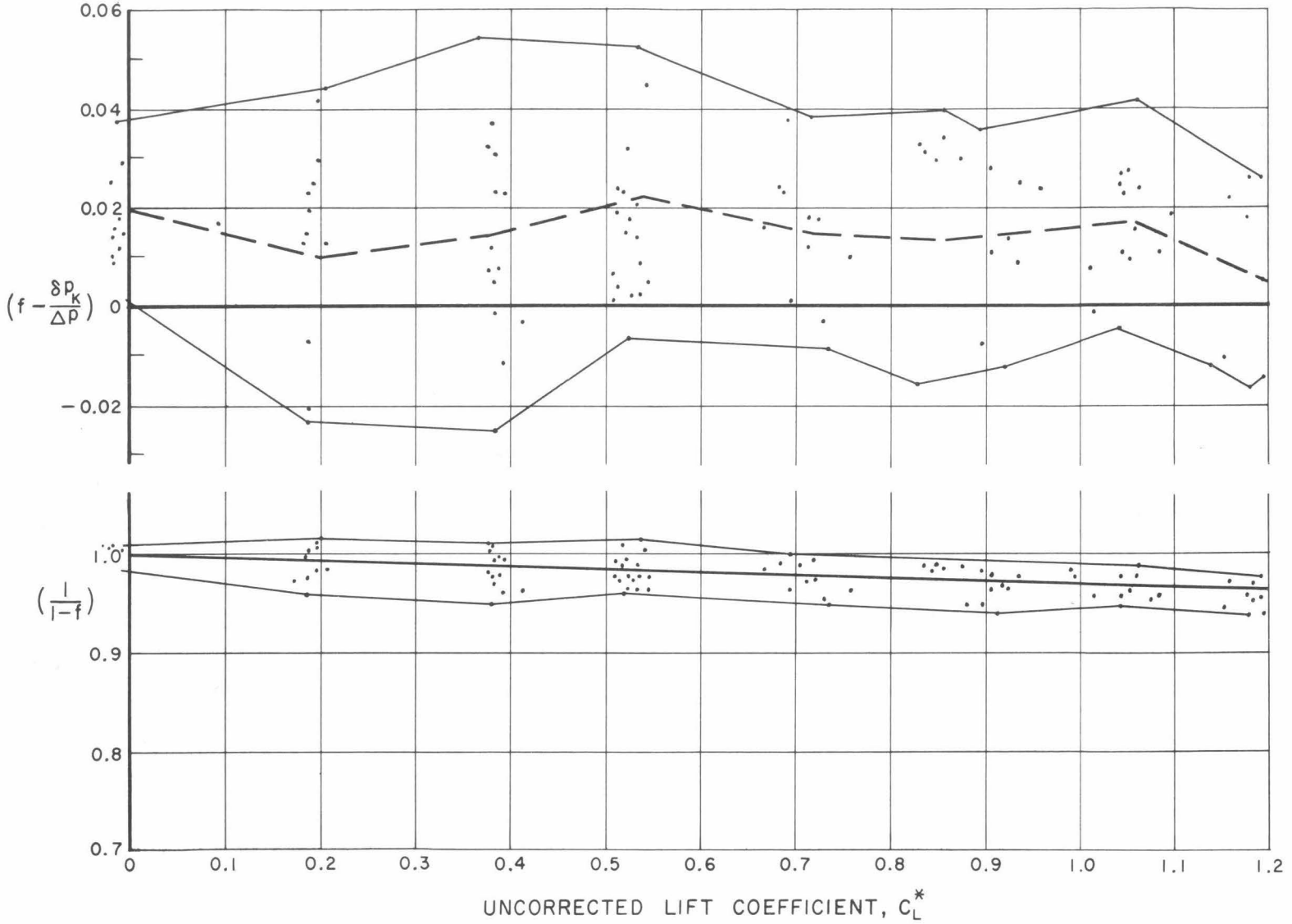

Figure A2.2 Model interference corrections for the force coefficients and the cavitation number.

TABLE I - CHARACTERISTICS OF HYDROFOIL IN NON-CAVITATING FLOW

V = 19.30 ft/sec.
Re = 0.46 x 10^6

α	C_L	C_D	C_M
-4.00	0.0004	0.0346	-0.1104
-2.00	0.1985	0.0197	-0.0463
0	0.3764	0.0147	-0.0007
2.00	0.5005	0.0186	0.0426
4.00	0.6603	0.0266	0.0845
6.00	0.8420	0.0478	0.1386
8.00	0.9628	0.0747	0.1819
10.00	1.0931	0.1180	0.2071
15.00	0.9366	-	0.0960
10.00	1.1027	0.1193	0.2083
8.00	0.9883	0.0774	0.1837
6.00	0.8370	0.0462	0.1342
4.00	0.7093	0.0278	0.0833
2.00	0.5101	0.0194	0.0380
0	0.3736	0.0133	-0.0111
-2.00	0.1961	0.0178	-0.0556
-4.00	-0.0021	0.0304	-0.1124

V = 25.93 ft/sec.
Re = 0.62 x 10^6

α	C_L	C_D	C_M
-4.00	-0.0022	0.0304	-0.1045
-3.50	0.0386	0.0266	-0.0923
-3.00	0.0941	0.0221	-0.0750
-2.50	0.1443	0.0192	-0.0625
-2.00	0.1907	0.0168	-0.0470
-1.50	0.2358	0.0154	-0.0374
-1.00	0.2776	0.0152	-0.0253
-0.50	0.3237	0.0139	-0.0138
0	0.3671	0.0135	-0.0039
0.50	0.4178	0.0124	0.0072
1.00	0.4619	0.0135	0.0180
1.50	0.4768	0.0158	0.0310
2.00	0.5122	0.0168	0.0424
2.50	0.5437	0.0180	0.0539
3.00	0.5920	0.0196	0.0652
3.50	0.6329	0.0222	0.0763
4.00	0.6763	0.0256	0.0877
6.00	0.8462	0.0464	0.1383
8.00	0.9953	0.0739	0.1883
10.00	1.1182	0.1193	0.2086
15.00	0.9574	-	0.1097
10.00	1.1265	0.1201	0.2137
8.00	0.9974	0.0734	0.1882
6.00	0.8577	0.0465	0.1416
4.00	0.6782	0.0253	0.0880
2.00	0.5055	0.0176	0.0342
0	0.3819	0.0123	-0.0092
-2.00	0.1964	0.0163	-0.0563
-4.00	-0.0028	0.0297	-0.1097

V = 31.17 ft/sec.
Re = 0.75 x 10^6

α	C_L	C_D	C_M
2.25	0.5317	0.0167	0.0439
2.00	0.5032	0.0159	0.0395
1.75	0.4928	0.0152	0.0322
1.50	0.4680	0.0145	0.0270
1.25	0.4574	0.0139	0.0218
1.00	0.4503	0.0125	0.0166
0.75	0.4541	0.0122	0.0116
0.50	0.4236	0.0133	0.0058
0.25	0.3965	0.0118	-0.0025
0	0.3837	0.0128	-0.0056
-0.25	0.3534	0.0131	-0.0117
-0.50	0.3335	0.0127	-0.0172
-0.75	0.3166	0.0130	-0.0241
-1.00	0.2907	0.0133	-0.0280
-1.25	0.2704	0.0139	-0.0345
-1.50	0.2453	0.0142	-0.0398
-1.75	0.2224	0.0153	-0.0471
-2.00	0.1982	0.0163	-0.0513
-2.25	0.1763	0.0173	-0.0576
-2.50	0.1506	0.0186	-0.0655
-2.75	0.1245	0.0198	-0.0725
-3.00	0.0981	0.0195	-0.0812
-3.50	0.0472	0.0255	-0.0943
-4.00	-0.0066	0.0306	-0.1097

V = 31.32 ft/sec.
Re = 0.75 x 10^6

α	C_L	C_D	C_M
-4.00	-0.0065	0.0309	-0.1053
-3.50	0.0487	0.0262	-0.0932
-3.00	0.0995	0.0223	-0.0782
-2.75	0.1247	0.0201	-0.0723
-2.50	0.1481	0.0190	-0.0665
-2.25	0.1721	0.0178	-0.0564
-2.00	0.1921	0.0164	-0.0476
-1.75	0.2140	0.0152	-0.0400
-1.50	0.2420	0.0149	-0.0375
-1.25	0.2636	0.0146	-0.0313
-1.00	0.2778	0.0136	-0.0244
-0.75	0.3106	0.0137	-0.0192
-0.50	0.3295	0.0131	-0.0140
-0.25	0.3583	0.0133	-0.0089
0	0.3714	0.0129	-0.0026
0.25	0.4023	0.0122	0.0016
0.50	0.4261	0.0119	0.0089
0.75	0.4478	0.0126	0.0148
1.00	0.4539	0.0138	0.0197
1.25	0.4490	0.0141	0.0245
1.50	0.4644	0.0152	0.0303
1.75	0.4781	0.0164	0.0356
2.00	0.5031	0.0164	0.0408
2.25	0.5349	0.0167	0.0474
2.50	0.5443	0.0172	0.0540
2.75	0.5725	0.0185	0.0593
3.00	0.5797	0.0184	0.0647
3.50	0.6360	0.0217	0.0775
4.00	0.6751	0.0245	0.0896
5.00	0.7732	0.0338	0.1151
6.00	0.8352	0.0447	0.1391
8.00	0.9873	0.0735	0.1858
10.00	1.0919	0.1182	0.2044
8.00	0.9993	0.0738	0.1880
6.00	0.8563	0.0450	0.1426
5.00	0.7763	0.0330	0.1188
4.00	0.6848	0.0244	0.0903
3.50	0.6260	0.0217	0.0777
3.00	0.5882	0.0193	0.0638
2.75	0.5688	0.0178	0.0567
2.50	0.5527	0.0174	0.0528
2.25	0.5245	0.0165	0.0489

TABLE II - CHARACTERISTICS OF HYDROFOIL IN CAVITATING FLOW

V = 30.33 ft/sec $\alpha = 4^\circ$

K_v	K	C_L	C_D	C_M
0.158	0.1165	0.1703	0.0271	0.0119
0.249	0.1825	0.2548	0.0269	0.0191
0.273	0.2367	0.2780	0.0280	0.0230
0.396	0.3132	0.4327	0.0313	0.0324
0.372	0.2940	0.3698	0.0299	0.0421
0.448	0.3605	0.4572	0.0322	0.0461
0.5000	0.4205	0.5314	0.0343	0.0739
0.5900	0.4945	0.6052	0.0344	-
0.6780	0.5723	0.7021	0.0362	-
0.7270	0.6279	0.7824	0.0369	0.0706
0.7550	0.6656	0.8162	0.0350	-
0.7920	0.6864	0.8763	0.0339	0.0770
0.809	0.6919	0.8886	0.0305	0.0781
0.856	0.7303	0.8630	0.0254	0.0903
0.933	0.7707	0.8216	0.0187	0.1045
0.906	0.8007	0.8203	0.0168	0.1074
0.963	0.8167	0.8065	0.0129	0.1117
0.916	0.8265	0.8233	0.0167	0.1078
0.979	0.8733	0.7917	0.0118	0.1135
1.032	0.9055	0.7478	0.0135	0.1091
2.130	1.625	0.6899	0.0194	0.0939

V = 30.61 ft/sec. $\alpha = 6^\circ$

K_v	K	C_L	C_D	C_M
0.229	0.2016	0.2503	0.0362	0.0318
0.348	0.2994	0.3383	0.0301	0.0423
0.454	0.3814	0.4516	0.0474	0.0496
0.585	0.5030	0.6060	0.0597	0.0589
0.650	0.5609	0.6825	0.0631	0.0645
0.834	0.7012	0.8795	0.0663	0.0797
0.961	0.8230	1.0335	0.0702	0.0934
1.052	0.9045	1.0898	0.0653	0.1084
1.108	0.9486	1.0617	0.0610	0.1200
1.285	1.1006	0.9994	0.0365	0.1583
1.337	1.1596	0.9830	0.0342	0.1639
1.509	1.2451	0.9440	0.0337	0.1633
1.565	1.3286	0.9197	0.0337	0.1593
1.738	1.4040	0.9026	0.0346	0.1520
1.805	1.4545	0.9002	0.0358	0.1534

V = 24.96 ft/sec. $\alpha = 6^\circ$

K_v	K	C_L	C_D	C_M
1.740	1.3405	0.8815	0.0362	0.1501
1.553	1.2847	0.9090	0.0357	0.1575
1.085	0.9075	1.0666	0.0649	0.1223
0.782	0.6411	0.7973	0.0670	0.0779
0.570	0.4541	0.5746	0.0564	0.0600
0.363	0.2898	0.3514	0.0355	0.0478
0.274	0.2053	0.2624	0.0316	0.0417

V = 19.29 ft/sec. $\alpha = 6^\circ$

K_v	K	C_L	C_D	C_M
1.751	1.3272	0.8959	0.0469	0.1307
1.363	1.0692	0.9856	0.0429	0.1363
1.173	0.9151	1.0635	0.0590	0.1104

V = 30.15 ft/sec. $\alpha = 8^\circ$

K_v	K	C_L	C_D	C_M
2.544	1.7636	1.0126	0.0624	0.1942
1.945	1.6058	1.0685	0.0627	0.2034
1.819	1.5295	1.0620	0.0608	0.2029
1.706	1.4153	1.0605	0.0612	0.2002
1.530	1.2988	1.0859	0.0730	0.1863
1.013	0.8481	1.0340	0.1140	0.0947
0.817	0.7071	0.8537	0.1051	0.0780
0.757	0.6345	0.7839	0.0994	0.0739
0.616	0.5027	0.6322	0.0857	0.0667
0.503	0.4191	0.5068	0.0713	0.0599
0.369	0.3069	0.3782	0.0526	0.0515
0.289	0.2416	0.3228	0.0172	0.0434

V = 24.78 ft/sec. $\alpha = 8^\circ$

K_v	K	C_L	C_D	C_M
2.060	1.6375	1.0374	0.0652	0.1975
1.942	1.5808	1.0574	0.0651	0.1989
0.914	0.7394	0.9376	0.1109	0.0874
0.538	0.4292	0.5462	0.0748	0.0653
0.412	0.3135	0.4044	0.0604	0.0565
0.326	0.2397	0.3301	0.0484	0.0504

V = 18.97 ft/sec. $\alpha = 8^\circ$

K_v	K	C_L	C_D	C_M
2.050	1.5704	1.0491	0.0664	0.1963
1.720	1.3899	1.0903	0.0701	0.2069
1.414	1.1253	1.1875	0.0930	0.1935
1.208	0.9769	1.1715	0.1149	0.1372
0.962	0.7475	0.9647	0.1123	0.0948
0.814	0.6223	0.7920	0.1005	0.0813
0.741	0.5292	0.6159	0.0866	0.0716
1.962	1.5238	1.0436	0.0688	0.2033
1.395	1.1201	1.1987	0.0943	0.1647
1.157	0.8636	1.2155	0.1122	0.1172
0.919	0.7373	0.9417	0.1100	0.0912

V = 31.42 ft/sec. $\alpha = 10^\circ$

K_v	K	C_L	C_D	C_M
0.786	0.6675	0.8011	0.1302	0.0793
0.733	0.6271	0.7583	0.1221	0.0774
0.396	0.3388	0.4427	0.0634	0.0518
0.318	0.2898	0.4109	0.0578	0.0338

V = 24.97 ft/sec. $\alpha = 10^\circ$

K_v	K	C_L	C_D	C_M
2.275	1.7196	1.1573	0.1067	0.2191
2.100	1.6397	1.1730	0.1100	0.2156
1.894	1.5245	1.2028	0.1170	0.2075
1.586	1.2959	1.2642	0.1411	0.1753
1.033	0.8616	1.1249	0.1652	0.0926
0.730	0.5728	0.7423	0.1225	0.0781
0.429	0.3643	0.4623	0.0790	0.0622
0.429	0.2707	0.3924	0.0769	0.0590

V = 18.90 ft/sec. $\alpha = 10^\circ$

K_v	K	C_L	C_D	C_M
2.304	1.6715	1.1324	0.1084	0.2189
2.041	1.5691	1.1680	0.1145	0.2172
1.919	1.5025	1.2086	0.1189	0.2120
1.568	1.2552	1.3014	0.1452	0.1863
1.379	1.1331	1.3274	0.1758	0.1414
1.336	1.0869	1.3138	0.1705	0.1348
1.117	0.9384	1.2206	0.1741	0.1024
0.966	0.8248	1.0615	0.1576	0.0960
0.818	0.7135	0.8680	0.1375	0.0878
1.345	1.0249	1.3094	0.1635	0.1374
1.103	0.8577	1.1344	0.1658	0.1018
0.973	0.7602	0.9726	0.1564	0.0938
0.647	0.4793	0.6219	0.1101	0.0758
0.552	0.3830	0.5125	0.0928	0.0765

DISTRIBUTION LIST FOR UNCLASSIFIED REPORTS AND PREPRINTS ISSUED UNDER CONTRACT Nonr 220(24) (NR 062-010)

Chief of Naval Research
Department of the Navy
Washington 25, D.C.
Attn: Codes 438 3
461 1
463 1
466 1

Commanding Officer
Office of Naval Research
Branch Office
495 Summer Street
Boston 10, Massachusetts 1

Commanding Officer
Office of Naval Research
Branch Office
207 West 24th Street
New York 11, New York 1

Commanding Officer
Office of Naval Research
Branch Office
1030 East Green Street
Pasadena, California 1

Commanding Officer
Office of Naval Research
Branch Office
1000 Geary Street
San Francisco 9, California 1

Commanding Officer
Office of Naval Research
Branch Office
Box 39, Navy No. 100
Fleet Post Office
New York, New York 25

Director
Naval Research Laboratory
Washington 25, D.C.
Attn: Code 2027 6

Chief, Bureau of Naval Weapons
Department of the Navy
Washington 25, D.C.
Attn: Codes RUAW-4 1
RRRE 1
RAAD 1
RAAD-222 1
DIS-42 1

Chief, Bureau of Ships
Department of the Navy
Washington 25, D.C.
Attn: Codes 310 1
312 1
335 1
420 1
421 1
440 1
442 1
449 1

Chief, Bureau of Yards and Docks
Department of the Navy
Washington 25, D.C.
Attn: Code D-400 1

Commanding Officer and Director
David Taylor Model Basin
Washington 7, D.C.
Attn: Codes 108 1
142 1
500 1
513 1
520 1
525 1
526 1
526A 1
530 1
533 1
580 1
585 1
589 1
591 1
591A 1
700 1

Commander
U.S. Naval Ordnance Test Station
China Lake, California
Attn: Code 753 1

Commander
U.S. Naval Ordnance Test Station
Pasadena Annex
3202 E. Foothill Blvd.
Pasadena, California 1
Attn: Code P-508 1

Commander
Planning Department
Portsmouth Naval Shipyard
Portsmouth, New Hampshire 1

Commander
Planning Department
Boston Naval Shipyard
Boston 29, Massachusetts 1

Commander
Planning Department
Pearl Harbor Naval Shipyard
Navy No. 128, Fleet Post Office
San Francisco, California 1

Commander
Planning Department
San Francisco Naval Shipyard
San Francisco 24, California 1

Commander
Planning Department
Mare Island Naval Shipyard
Vallejo, California 1

Commander
Planning Department
New York Naval Shipyard
Brooklyn 1, New York 1

Commander
Planning Department
Puget Sound Naval Shipyard
Bremerton, Washington 1

Commander
Planning Department
Philadelphia Naval Shipyard
U.S. Naval Base
Philadelphia 12, Pennsylvania 1

Commander
Planning Department
Norfolk Naval Shipyard
Portsmouth, Virginia 1

Commander
Planning Department
Charleston Naval Shipyard
U.S. Naval Base
Charleston, South Carolina 1

Commander
Planning Department
Long Beach Naval Shipyard
Long Beach, California 1

Commander
Planning Department
U.S. Naval Weapons Laboratory
Dahlgren, Virginia 1

Commander
U.S. Naval Ordnance Laboratory
White Oak, Maryland 1

Dr. A.V. Hershey
Computation and Exterior
Ballistics Laboratory
U.S. Naval Weapons Laboratory
Dahlgren, Virginia 1

Superintendent
U.S. Naval Academy
Annapolis, Maryland
Attn: Library 1

Superintendent
U.S. Naval Postgraduate School
Monterey, California 1

Commandant
U.S. Coast Guard
1300 E. Street, N.W.
Washington, D.C. 1

Secretary Ship Structure Committee
U.S. Coast Guard Headquarters
1300 E Street, N.W.
Washington, D.C. 1

Commander
Military Sea Transportation Service
Department of the Navy
Washington 25, D.C. 1

U.S. Maritime Administration
GAO Building
441 G Street, N.W.
Washington, D.C.
Attn: Division of Ship Design 1
Division of Research 1

Superintendent
U.S. Merchant Marine Academy
Kings Point, Long Island, New York
Attn: Capt. L.S. McCready (Dept.
of Engineering) 1

Commanding Officer and Director
U.S. Navy Mine Defense Laboratory
Panama City, Florida 1

Commanding Officer
NROTC and Naval Administrative Unit
Massachusetts Institute of Technology
Cambridge 39, Massachusetts 1

U.S. Army Transportation Research and Development Command
Fort Eustis, Virginia
Attn: Marine Transport Division 1

Mr. J.B. Parkinson
National Aeronautics and Space Administration
1512 H Street, N.W.
Washington 25, D.C. 1

Director
Langley Research Center
Langley Station
Hampton, Virginia
Attn: Mr. I.E. Garrick 1
Mr. D.J. Marten 1

Director Engineering Sciences Division
National Science Foundation
1951 Constitution Avenue, N.W.
Washington 25, D.C. 1

Director
National Bureau of Standards
Washington 25, D.C.
Attn: Fluid Mechanics Division
Dr. G.B. Schubauer 1
Dr. G.H. Keulegan 1
Dr. J.M. Franklin 1

Defense Documentation Center
Cameron Station
Alexandria, Virginia 20

Office of Technical Services
Department of Commerce
Washington 25, D.C. 1

California Institute of Technology
Pasadena, California
Attn: Professor M.S. Plesset 1
Professor T.Y. Wu 1
Professor A.J. Acosta 1

University of California
Department of Engineering
Los Angeles 24, California
Attn: Dr. A. Powell 1

Director
Scripps Institute of Oceanography
University of California
La Jolla, California 1

Professor M.L. Albertson
Department of Civil Engineering
Colorado A. and M. College
Fort Collins, Colorado 1

Professor J.E. Cermak
Department of Civil Engineering
Colorado State University
Fort Collins, Colorado 1

Professor W.R. Sears
Graduate School of Aeronautical Engrg.
Cornell University
Ithaca, New York 1

State University of Iowa
Iowa Institute of Hydraulic Research
Iowa City, Iowa
Attn: Dr. H. Rouse 1
Dr. L. Landweber 1

Harvard University
Cambridge 38, Massachusetts
Attn: Professor G. Birkhoff 1
(Department of Mathematics)
Professor G.F. Carrier 1
(Department of Mathematics)

Massachusetts Institute of Technology
Cambridge 39, Massachusetts
Attn: Dept. of Naval Architecture and Marine Engineering 1
Professor A.T. Ippen 1

University of Michigan
Ann Arbor, Michigan
Attn: Professor R.B. Couch 1
(Dept. of Naval Architecture)
Professor W.W. Willmarth 1
(Aero.Engrg. Dept.)
Professor M.S. Uberoi 1
(Aero.Engrg. Dept.)

Dr. L.G. Straub, Director
St. Anthony Falls Hydraulic Laboratory
University of Minnesota
Minneapolis 14, Minnesota 1
Attn: Mr. J.N. Wetzel 1
Professor B. Silberman 1

Professor J.J. Foody
Engineering Department
New York State University Maritime College
Fort Schulyer, New York 1

New York University
Institute of Mathematical Sciences
25 Waverly Place
New York 3, New York
Attn: Professor J. Keller 1
Professor J.J. Stoker 1

The Johns Hopkins University
Department of Mechanical Engineering
Baltimore 18, Maryland
Attn: Professor S. Corrsin 1
Professor O.M. Phillips 2

Massachusetts Institute of Technology
Dept. of Naval Architecture and
Marine Engineering
Cambridge 39, Massachusetts
Attn: Professor M.A. Abkowitz 1

Dr. G.F. Wislicenus
Ordnance Research Laboratory
Pennsylvania State University
University Park, Pennsylvania 1
Attn: Dr. M. Sevik 1

Professor R.C. DiPrima
Department of Mathematics
Rensselaer Polytechnic Institute
Troy, New York 1

Stevens Institute of Technology
Davidson Laboratory
Castle Point Station
Hoboken, New Jersey
Attn: Mr. D. Savitsky 1
Mr. J.P. Breslin 1
Mr. C.J. Henry 1
Mr. S. Tsakonas 1

Webb Institute of Naval Architecture
Crescent Beach Road
Glen Cove, New York
Attn: Professor E.V. Lewis 1
Technical Library 1

Director
Woods Hole Oceanographic Institute
Woods Hole, Massachusetts 1

Executive Director
Air Force Office of Scientific Research
Washington 25, D.C.
Attn: Mechanics Branch 1

Commander
Wright-Patterson Air Force Base, Ohio
Wright Air Development Division
Aircraft Laboratory
Attn: Mr. W. Mykytow,
Dynamics Branch 1

Cornell Aeronautical Laboratory
4455 Genesee Street
Buffalo, New York
Attn: Mr. W. Targoff 1
Mr. R. White 1

Massachusetts Institute of Technology
Fluid Dynamics Research Laboratory
Cambridge 39, Massachusetts
Attn: Professor H. Ashley 1
Professor M. Landahl 1
Professor J. Dugundji 1

Hamburgische Schiffbau-Versuchsanstalt
Bramfelder Strasse 164
Hamburg 33, Germany
Attn: Dr. O. Grim 1
Dr. H.W. Lerbs 1
Dr. H. Schwanecke 1

Institut fuer Schiffbau der
Universitaet Hamburg
Berliner Tor 21
Hamburg 1, Germany
Attn: Prof. G.P. Weinblum, Dir. 1

Transportation Technical Research
Institute
1-1057, Mejiro-Cho, Toshima-Ku
Tokyo, Japan 1

Max-Planck Institut fuer Stroemungs-
forschung
Bottingerstrasse 6/8
Goettingen, Germany
Attn: Dr. H. Reichardt 1

Hydro-og Aerodynamisk Laboratorium
Lyngby, Denmark
Attn: Professor Carl Prohaska 1

Skipsmodelltanken
Trondheim, Norway
Attn: Professor J.K. Lunde 1

Versuchsanstalt fuer Wasserbau
und Schiffbau
Schleuseninsel im Tiergarten
Berlin, Germany
Attn: Dr. S. Schuster, Director 1
Dr. Grosse 1

Technische Hogeschool
Institut voor Toegepaste Wiskunde
Julianalaan 132
Delft, Netherlands
Attn: Professor R. Timman 1

Bureau d'Analyse et de Recherche
Appliquees
47 Avenue Victor Cresson
Issy-Les-Moulineaux
Seine, France
Attn: Professor Siestrunck 1

Netherlands Ship Model Basin
Wageningen, The Netherlands
Attn: Dr. Ir. J.D. van Manen 1

National Physical Laboratory
Teddington, Middlesex, England
Attn: Mr. A. Silverleaf, Superintendent
Ship Division 1
Head, Aerodynamics Div. 1

Head, Aerodynamics Department
Royal Aircraft Establishment
Farnborough, Hants, England
Attn: Mr. M.O.W. Wolfe 2

Dr. S.F. Hoerner
148 Busteed Drive
Midland Park, New Jersey 1

Boeing Airplane Company
Seattle Division
Seattle, Washington
Attn: Mr. M.J. Turner 1

Electric Boat Division
General Dynamics Corporation
Groton, Connecticut
Attn: Mr. R. McCandliss 1

General Applied Sciences Labs. Inc.
Merrick and Stewart Avenues
Westbury, Long Island, New York 1

Gibbs and Cox, Inc.
21 West Street
New York, New York 1

Grumman Aircraft Engineering Corp.
Bethpage, Long Island, New York
Attn: Mr. E. Baird 1
Mr. E. Bower 1
Mr. W.P. Carl 1

Lockheed Aircraft Corporation
Missiles and Space Division
Palo Alto, California
Attn: Mr. R.W. Kermeen 1

Midwest Research Institute
425 Volker Blvd.
Kansas City 10, Missouri
Attn: Mr. Zeydel 1

Director, Dept. of Mechanical Sciences
Southwest Research Institute
8500 Culebra Road
San Antonio 6, Texas
Attn: Dr. H.N. Abramson 1
Mr. G. Ransleben 1
Editor, Applied Mechanics
Review 1

Convair
Div. of General Dynamics
3165 Pacific Highway
San Diego 12, California
Attn: Mr. R.H. Oversmith 1
Mr. H.T. Brooke 1

Hughes Tool Company
Aircraft Division
Culver City, California
Attn: Mr. M.S. Harned 1

Hydronautics, Incorporated
Pindell School Road
Howard County
Laurel, Maryland
Attn: Mr. Phillip Eisenberg 1

Rand Development Corporation
13600 Deise Avenue
Cleveland 10, Ohio
Attn: Dr. A.S. Iberall 1

U.S. Rubber Company
Research and Development Dept.
Wayne, New Jersey
Attn: Mr. L.M. White 1

Technical Research Group, Inc.
Route 110
Melville, New York
Attn: Mr. Jack Kotik 1

Mr. C. Wigley
Flat 102
6-9 Charterhouse Square
London, E.C. 1, England 1

AVCO Corporation
Lycoming Division
1701 K Street, N.W.
Apt. No. 904
Washington, D.C.
Attn: Mr. T.A. Duncan 1

Mr. J.G. Baker
Baker Manufacturing Company
Evansville, Wisconsin 1

Curtiss-Wright Corporation Research Division
Turbomachinery Division
Quehanne, Pennsylvania
Attn: Mr. George H. Pedersen 1

Dr. Blaine R. Parkin
AiResearch Manufacturing Corporation
9851-9951 Sepulveda Boulevard
Los Angeles 45, California 1

The Boeing Company
Aero-Space Division
Seattle 24, Washington
Attn: Mr. R.E. Bateman 1
(Internal Mail Station 46-74)

Lockheed Aircraft Corporation
California Division
Hydrodynamics Research
Burbank, California
Attn: Mr. Bill East 1

National Research Council
Montreal Road
Ottawa 2, Canada
Attn: Mr. E.S. Turner 1

The Rand Corporation
1700 Main Street
Santa Monica, California
Attn: Technical Library 1

Stanford University
Dept. of Civil Engineering
Stanford, California
Attn: Dr. Byrne Perry 1
Dr. E.Y. Hsu 1

Dr. Hirsh Cohen
IBM Research Center
P.O. Box 218
Yorktown Heights, New York 1

Mr. David Wellinger
Hydrofoil Projects
Radio Corporation of America
Burlington, Massachusetts 1

Food Machinery Corporation
P.O. Box 367
San Jose, California
Attn: Mr. G. Tedrew 1

Dr. T.R. Goodman
Oceanics, Inc.
Technical Industrial Park
Plainview, Long Island, New York 1

Professor Brunelle
Dept. of Aeronautical Engineering
Princeton University
Princeton, New Jersey 1

Commanding Officer
Office of Naval Research
Branch Office
230 N. Michigan Avenue
Chicago 1, Illinois 1

Morris Machine Works
Baldwinsville, New York
Attn: Mr. Fred F. Antunes
Hydraulic Engineer 1

Mr. R. Dean
Monsanto Chemical Company
800 N. Lindberg Boulevard
St. Louis 66, Missouri 1

Professor H.G. Flynn
Department of Electrical Engineering
College of Engineering
The University of Rochester
River Campus Station
Rochester 20, New York 1

Rocketdyne
6633 Canoga Avenue
Canoga Park, California
Attn: Librarian, Dept. 596-3 1

Professor J. William Holl
Dept. of Aeronautical Engineering
Pennsylvania State University
Ordnance Research Laboratory
P.O. Box 30
State College, Pennsylvania 1